Fermi National Accelerator Laboratory

FN-438
0400.000

Longitudinal Instabilities and Stability Criteria*

King-Yuen Ng

Fermi National Accelerator Laboratory
P.O. Box 500
Batavia, IL 60510

October 1986

*(To be published as a chapter in *Principles of High Energy Hadron Colliders, Part II, the Tevatron*, H. Edwards and M. Month, eds.)

Operated by Universities Research Association Inc. under contract with the United States Department of Energy

FN 438
0400.000

LONGITUDINAL INSTABILITIES AND STABILITY CRITERIA*

King-Yuen Ng

Fermi National Accelerator Laboratory+
Batavia, IL 60555

October, 1986
(First draft: May, 1986)

CONTENT

*To be published as a chapter in "Principles of High Energy Hadron Colliders", Part II, the Tevatron, edited by H. Edwards and M. Month.

+Operated by the Universities research Association, Inc., under contract with the U.S. Department of Energy.

12 LONGITUDINAL INSTABILITIES AND STABILITY CRITERIA

12.1 Criteria For Longitudinal Microwave Instability

The electromagnetic fields emitted by a particle beam will interact with the beam itself directly or indirectly through bouncing back from the walls of the vacuum chamber. For a beam with uniform longitudinal density, there is no longitudinal field and no force acting on the particles. However, if a small bump is introduced, it will produce a longitudinal space-charge force $eE = -e\partial\lambda/\partial\theta$ acting in the direction away from the bump, where λ is the local linear charge density and θ is the azimuthal angle around the accelerator ring (Fig. 12.1.1). This force will increase the energy at the front of the bump and decrease the energy at the back. However, above transition, this implies decreasing the revolution frequency at the front and increasing it at the back; the bump will increase in magnitude. In other words, any small local perturbation in the uniform density of the beam will grow resulting in a nonuniform particle distribution.

The growth rate can be easily derived for any longitudinal force even if it is not due to space charge[12.1.1]. We start from a beam with uniform linear density λ_o and fixed energy E. Let us assume a small perturbation λ_1 of harmonic n and collective frequency $\Omega/2\pi$. We write the density as

$$\lambda(\theta,t) = \lambda_o + \lambda_1 e^{-j(n\theta-\Omega t)}. \tag{12.1.1}$$

Because of the continuity equation

$$\frac{\partial\lambda}{\partial t} + \frac{\partial}{\partial\theta}(\lambda\omega) = 0, \tag{12.1.2}$$

the revolution frequency $\omega(\theta,t)/2\pi$ must be of the form

$$\omega(\theta,t) = \omega_o + \omega_1 e^{-j(n\theta-\Omega t)}, \tag{12.1.3}$$

where the deviation ω_1 from the unperturbed value ω_o is given by

$$\omega_1 = (\Omega/n - \omega_o)\lambda_1/\lambda_o. \tag{12.1.4}$$

The current is given by $I(\theta,t) = \lambda(\theta,t)\omega(\theta,t)$ or

$$I(\theta,t) = I_o + I_1 e^{-j(n\theta-\Omega t)}, \tag{12.1.5}$$

with $I_1 = (\Omega/n)\lambda_1$. In above, only first-order quantities have been retained.

Riding on a particle with angular velocity ω_o, we should not see any change in revolution frequency except for that due to a longitudinal electric field from the beam particles bouncing from the walls. Thus, $d\omega/dt$ is

$$\partial\omega/\partial t + (\partial\omega/\partial\theta)(d\theta/dt) = (\partial\omega/\partial E)(dE/dt), \qquad (12.1.6)$$

where $\partial\omega/\partial E = -\eta\omega_o/\beta^2 E$ with $\eta = \gamma_t^{-2} - \gamma^{-2}$ denoting the frequency dispersion parameter, β the particle velocity relative to c the speed of light, $\gamma^2 = 1/(1-\beta^2)$, and γ_t is gamma at transition. The rate of increase in energy is $dE/dt = -eI_1 Z_L \omega_o/2\pi$, where Z_L, the longitudinal impedance per turn around the accelerator ring at harmonic n, is defined as the potential drop around the ring per unit current of harmonic n. We therefore have

$$j(\Omega - n\omega_o)\omega_1 = \eta e I_1 Z_L \omega_o^2/2\pi\beta^2 E. \qquad (12.1.7)$$

Equation (12.1.7) has a physical meaning. As a result of the longitudinal impedance, we can imagine n buckets created each with peak voltage $-I_1 Z_L$. The particles trapped inside a bucket will execute synchrotron oscillation with

$$\omega_s^2 = -j\eta n e I_1 Z_L \omega_o^2/2\pi\beta^2 E. \qquad (12.1.8)$$

In above, a factor j has been inserted to take into account of the fact that, to produce buckets encircling the ripples or small bunches in the beam current, the voltage has to be 90^o out of phase. Riding on a particle with angular velocity ω_o, the particles inside one of those buckets will move, on the average, an azithumal angle of π/n across the bucket in time π/ω_s (half an oscillation); or they have an angular velocity of $\omega \sim (\omega_s/n)\exp(j\omega_s t)$. Thus, the rate of change of angular velocity is

$$d\omega/dt = j\omega_s^2/n, \qquad (12.1.9)$$

which is the same as Eq. (12.1.7).

Substituting Eq. (12.1.4) for ω_1, noting that $I_o = \lambda_o\omega_o$, and letting $\Omega/n \sim \omega_o$, we get for the collective frequency

$$(\Omega - n\omega_o)^2 = -jn\eta e I_o Z_L \omega_o^2/2\pi\beta^2 E. \qquad (12.1.10)$$

This gives the shift in revolution frequency; the imaginary part of Ω, if negative, gives the rate of growth for the wave at harmonic n. Note that I_o appears in the formula, although it is I_1 that excites the longitudinal electric field. This is because this electric field interacts with every particle in the beam.

However, if the beam particles have an energy spread ΔE corresponding to a revolution frequency spread $\Delta\omega = -\eta\omega_o\Delta E/\beta^2 E$, the collective effect cannot take place or the coherence of the perturbing wave will be destroyed when the growth time $-1/\mathrm{Im}\Omega$ is bigger than $2/n\Delta\omega$, the time for one wavelength to go out of phase by 180^o. In other words, the beam is stable when

$$4|\eta e I_o Z_L \omega_o^2/2\pi nE| \leq (\eta \omega_o \Delta E/\beta^2 E)^2. \qquad (12.1.11)$$

This is the famous Keil-Schnell criterion for microwave stability for a coasting beam[12.1.2].

For a single bunch, if the bunch length is much longer than the wavelength of the perturbation and the synchrotron oscillation period is much longer than the growth time, the bunch, at least its central portion, resembles a coasting beam during the unstable growth. Therefore, the above Keil-Schnell criterion applies if we replace the average total current I_o by the local peak current I_p; i.e.,

$$\left|\frac{Z_L}{n}\right| \leq \frac{2\pi|\eta|E/e}{\beta^2 I_p}\left(\frac{\sigma_E}{E}\right)^2. \qquad (12.1.12)$$

In the above, we have written the RMS energy spread σ_E instead of $\Delta E/2$, because this is the exact criterion for a Gaussian bunch when a careful derivation is performed using the linearized Vlasov equation[12.1.3]. The peak current is $I_p = 1/\sqrt{2\pi}\sigma_\tau$, where σ_τ is the RMS time spread of the bunch. The Vlasov equation leads to a dispersion relation which can be plotted as growth-rate contours in the $(\Delta\Omega_o/n)^2$-plane, where $\Delta\Omega_o = \Omega - n\omega_o$, given by Eq. (12.1.10), is the frequency shift without Landau damping. Such a plot is given in Fig. 12.1.2, where only the stability contour is shown. A given Z_L/n corresponds to a point in the $(\Delta\Omega_o/n)^2$-plane. If the point lies outside the stability contour, there exists at least one growing solution and the bunch will be unstable. If the point lies inside the stability contour, all solutions are stable. Noticing that $(\Delta\Omega_o/n)^2$ is proportional to $-j\eta Z_L/n$, above transition when $\eta > 0$, the criterion of Eq. (12.1.12) corresponds to the point A, where the impedance is capacitive. An inductive Z_L/n lies on the positive vertical axis and is therefore always stable. A real Z_L/n corresponds to the point B which is ~1.434 times farther away from the origin than the point A, (for Gaussian bunch only). Therefore, when the impedance is real, the stability criterion of Eq. (12.1.12) can be relaxed by inserting the factor 1.434 on the right side. Below transition when $\eta < 0$, a capacitive impedance, corresponding to a point on the positive vertical axis, will always be stable, while an inductive one, corresponding to a point on the negative vertical axis, can be unstable if it is too big.

As stated above, the longitudinal electric field produced by the impedance interacts on every particle of the bunch. The impedance Z_L in the above criterion is therefore the convolution of the impedance $Z(\omega)$ of the ring and the frequency spectrum $\rho(\omega)$ of the bunch

$$Z_L = \int Z(n\omega_o+\omega)\rho(\omega)d\omega; \qquad (12.1.13)$$

$\rho(\omega)$ being normalized to unity. When the impedance is a broad band much broader than σ_τ^{-1}, the frequency spread of the bunch, the convolu-

tion depends only on the peak of the broad-band impedance, and therefore Z_L in Eq. (12.1.12) represents the peak impedance of a broad band. However, with cavities and pipe-joining housings along the vacuum chamber, the impedance may exhibit sharp resonances with frequency much narrower than that of the bunch. For a narrow resonance of shunt impedance Z_{sh}, quality factor Q, and resonance frequency $\omega_R \sim n\omega_o$, the convolution gives

$$Z_L = [\sigma_\tau/\sqrt{2\pi}]\,[(\pi\omega_R/2)(Z_{sh}/Q)], \tag{12.1.14}$$

where the first term is the peak value of the bunch spectrum ρ and the second the area under the narrow resonance. This is just the effective impedance seen by the bunch, which, because of its finite frequency spread, is not able to resolve the narrow peak. Substituting this into Eq. (12.1.12), we obtain a criterion for narrow resonances[12.1.4]

$$\frac{Z_{sh}}{Q} \le \frac{4|\eta|E/e}{\beta^2 I_{AV}}\left(\frac{\sigma_E}{E}\right)^2, \tag{12.1.15}$$

where $I_{AV} = eN\omega_o/2\pi$ is the average current of the bunch containing N particles.

12.2 Stability Limits

In this section we try to estimate the limits[12.2.1] of Z_L/n or Z_{sh}/Q for the Main Ring in order to ensure longitudinal instability during its different performances.

The present duties of the Main Ring are:

(1) To accelerate proton (or antiproton) bunches up to 150 GeV and coalesce 7 to 13 of them to form an intense bunch of $\sim 10^{11}$ to be injected into the Energy Saver for further acceleration and eventual collision with an antiproton (proton) bunch. In order to achieve a high luminosity, the initial bunches must be kept at small bunch areas ~0.2 eV-sec before coalescence.

(2) To accelerate intense proton bunches up to 120 GeV for antiproton production. To maximize the production efficiency, these bunches must be of high intensity $\sim 2.4\times 10^{10}$ p/bunch and small bunch area ~0.2 eV-sec.

We see that, in each performance, the bunch area has to be small, unlike the operation in the fixed target mode where the bunch area was deliberately increased by the bunch spreader in order to achieve a better duty cycle.

Across transition

When the bunches are accelerated through transition, which corresponds to $\gamma_t = 18.75$, the frequency dispersion parameter η changes from negative to positive through zero. Equation (12.1.10) tells us that

there must be a portion of time that the bunch is unstable. The total growth across transition is[12.2.1] $G = \exp(S_a+S_b)$ where

$$S_{b,a} = \int \mathrm{Im}\Omega dt \tag{12.2.1}$$

represents the integration of the positive growth rate $\mathrm{Im}\Omega$ before and after transition. The rate of growth is dependent on the number of particles in the bunch N and also the driving impedance Z_L/n. The time t_o from loss of stability to transition or from transition to regain of stability is also dependent on NZ_L/n. In fact, it turns out that S_b+S_a scales as $(Z_L/n)^2N^2A^{-9/4}$, where $A = 6\pi\sigma_\tau\sigma_E$ is the bunch area. If space-charge is neglected, we have

$$\frac{S_b}{n} = \frac{S_a}{n} = \frac{F_1[eN(Z_L/n)\gamma_t]^2(E_o/e)^2\sigma_\tau}{V_{RF}\sin\phi_o(A/e)^3}, \tag{12.2.2}$$

where γ_t is gamma at transition, V_{RF} is the RF voltage at transition, ϕ_o is the synchronized phase at transition, E_o is the rest energy of the particle concerned, σ_τ is the RMS time spread of the bunch at the moment when stability is lost (before transition) or when stability is regained (after transition), and $F_1 = 8.735$ is a numerical constant. The RMS time spread σ_τ in above can be evaluated from

$$\frac{\sigma_\tau}{T} = \frac{2}{3^{1/3}\Gamma(\frac{1}{3})}\left[\frac{AeV_{RF}\omega_o\sin\phi_o}{6\pi E_o^2\beta^2\gamma_t^4}\right]^{1/2}\left[1+0.686\left|\frac{t_o}{T}\right|\right] \tag{12.2.3}$$

for $|t_o/T| \ll 1$, and

$$\frac{\sigma_\tau}{T} = \left[\frac{AeV_{RF}\omega_o\sin\phi_o}{6\pi^2E_o^2\beta^2\gamma_t^4}\right]^{1/2}\left|\frac{t_o}{T}\right|^{1/4} \tag{12.2.4}$$

for $|t_o/T| \gg 1$. In above, ω_o is the angular revolution frequency of the bunch and β its velocity in unit of c, the light velocity. The characteristic time

$$T = \left[\frac{4\pi^2(E_o/e)^2\beta^2\gamma_t^4}{h\omega_o^3V_{RF}^2\sin 2\phi_o}\right]^{1/3}, \tag{12.2.5}$$

where h is the RF harmonic, is a measure of the time for which the bucket change is not adiabatic. The time t_o is given by

$$|t_o| = \frac{F_2eN(Z_L/n)\gamma_t^4(E_o/e)^2\sigma_\tau}{\omega_oV_{RF}\sin\phi_o(A/e)^2}, \tag{12.2.6}$$

where $F_2 = 49.42$ is a constant.

For $N = 1.2\times10^{10}$, $Z_L/n = 10$ ohms, $A = 0.15$ eV-sec, RF voltage $V_{RF} = 2.5$ MV, and a synchronous phase $\phi_o = 50^o$, we get $2t_o = 5.2$ ms and $(S_b+S_a)/n = 3.6\times10^{-5}$. Exact numerical solution[12.2.2] of the dispersion relation including space-charge effects gives 5.5 ms and 3.86×10^{-5}. The characteristic time T is 2.86 ms. Microwave signals at 1.65 GHz have been observed (see Section 12.5 below) corresponding to an harmonic of $n = 3.46\times10^4$. Thus, the growth across transition is $G \sim 3.86$ times. However, this is the growth of only the microwave amplitude, the perturbing one that we discussed in Section 12.1. It will increase the energy spread and dilute the bunch area through second order effects. The relation between the growth of the bunch area and that of the microwave signal is complicated and model-dependent and will be presented elsewhere. But, in some sense, we can consider $G = \exp(S_b+S_a)$ as a measure of the growth of the bunch area. The final size of the microwave amplitude depends on the the size of that amplitude before transition. In our case, the RMS bunch length σ_τ near transition is ~0.3 ns or the RMS frequency spread is $\sigma_\omega \sim 3.3$ GHz. Thus, the amplitude at $\omega/2\pi = 1.65$ GHz is only $\exp(-\omega^2/2\sigma_\omega^2)$ or 0.72% of the amplitude a low frequencies. Thus, a growth of 3.86 times may not be very much. However, if the bunch is ill-behaved and does not fit the bucket well at the beginning, its amplitude in the microwave region can be comparable to the amplitude at low frequencies and a growth of 3.86 times may be very significant. Growth of bunch area across transition in the Main Ring has been reported to be 20% to ~4 times. We believe that this variation is mainly due to the behavior of the bunch before transition.

When the Main Ring accelerates proton bunches for $\bar{p}$ production, the number of protons per bunch $N \sim 2.4\times10^{10}$ is bigger and the bunch area. According to the scaling law, S_b+S_a increases by four times and the growth of the microwave amplitude becomes $G = 146$. If the bunch area is smaller to start with, the growth may become too big to tolerate. But, so far we have included linear effects. Generally, nonlinear effects will come in causing overshoots and the growth will end.

Acceleration

After passing through transition, if we assume that the RF voltage V_{RF} and the synchronous phase ϕ_o are changed adiabatically and the bunch area $A = 6\pi\sigma_\tau\sigma_E$ is small compared with the bucket area, from Eq. (12.1.10), the Z_L/n limit becomes

$$\left|\frac{Z_L}{n}\right| = F\left(\frac{h}{I_o\beta}\right)^{1/4}\left(\frac{Ac}{R}\right)^{3/2}\left(\frac{\eta}{E}\right)^{3/4}\left(V_{RF}\cos\phi_o\right)^{1/4}, \qquad (12.2.7)$$

where $F = 3^{-3/2}(2\pi)^{-5/4}$, $h = 1113$, the harmonic number of the RF, $R = 1$ km the average radius of the main ring, I_o the average current of the bunch, and c the velocity of light. In deriving Eq. (12.2.2), use

has been made of the approximate relation between the RMS time spread σ_τ and RMS energy spread σ_E of the bunch; i.e.,

$$\sigma_\tau = (R/h\beta c)(|\eta|h/\nu_s)(\sigma_E/\beta^2 E), \qquad (12.2.8)$$

where $\nu_s = |h\eta V_{RF}\cos\phi_o/2\pi\beta^2 nE|^{1/2}$ is the synchrotron tune. After transition, η becomes bigger and bigger and $|V_{RF}\cos\phi_o|$ still increases; thus the bunch becomes more and more stable. Later, for higher energies, η approaches a constant and $|V_{RF}\cos\phi_o|$ is constant or decreasing; thus the $|Z_L/n|$ limit becomes smaller as the energy E increases. Figure 12.2.1 shows a typical acceleration cycle. We see that the limit is most stringent at the highest energy of 120 GeV or 150 GeV. Therefore, we need to discuss stability at these top energies only.

Bunch coalescence

Seven proton bunches each of intensity $N = 1.2\times10^{10}$ and area A = 0.20 eV-sec (we assume that the bunch area increases to 0.20 eV-sec across transition) at 150 GeV are allowed to coalesce into one bunch of intensity $\sim8\times10^{10}$. The procedure consists of lowering the RF voltage adiabatically from ~1.5 MV to ~2.30 kV so that the bunch will just fill the bucket. This h = 1113 RF is then turned off while a h = 53 RF of 22 kV is turned on. The 7 bunches will lie inside the h = 53 RF bucket and is allowed to rotate for 90°. This RF is then replaced by a h = 1113 RF of 0.46 MV to capture the 7 bunches into a single bucket. The RF is then increased slowly to 1 MV so that the coalesced high-intensity bunch is matched to the bucket. The $|Z_L/n|$ limit of each stage during the coalescence is listed in Table 12.2.1. We see that the lowest limit is $|Z_L/n| = 6.84\ \Omega$ for a broad band and $Z_{sh}/Q = 9.45\ k\Omega$ for a narrow resonance. This occurs when the RF voltage is lowered adiabatically to match the bunch. With the desire to obtain higher luminosity, sometimes up to 11 or 13 bunches are coalesced. However, under such conditions, a h = 106 RF is added alongside the h = 53 RF so as to linearize the 90° rotation and ensure a more efficient capture.

The antiprotons are coalesced at 150 GeV similarly. The only difference is that 13 adjacent bunches each of intensity $\sim8\times10^{9}$ are involved. Because of the lower intensity, the higher limit $|Z_L/n| = 10.3\ \Omega$ or $Z_{sh}/Q = 14.0\ k\Omega$ are obtained. This and other data are listed in Table 12.2.2

Preparation of p-bunches for $\bar{p}$ production

For fixed $\bar{p}$ momentum spread, the bunch area of the $\bar{p}$ is minimized by making the time spread of the bombarding proton bunches as narrow as possible. At the 120 GeV flat-top, the RF voltage is maintained at 4 MV and the bunches, about 0.2 eV-sec and intensity 2.4×10^{10}, are matched to the large bucket ($\Delta E \sim 300$ MeV). The RF is reduced to ~300 kV within two turns. The now mismatched bunches begin phase oscillation which results in a maximum time spread of $\sqrt{6}\sigma_\tau \sim 4$ ns, about half the bucket length. The RF is next increased quickly again

to its maximum value of 4 MV, whereupon the mismatched bunches rotate in one quarter phase oscillation to a large energy spread and narrow time spread configuration ($\sqrt{6}\sigma_\tau \sim 0.3$ ns) and are extracted. The various bunch parameters and $|Z_L/n|$ limits are summarized in Table 12.2.3. We see that $|Z_L/n|$ reaches 6.61 Ω when the time spread of the proton bunch is biggest. For a sharp resonance narrower than the bunch spectrum, this corresponds to $Z_{sh}/Q = 21.4$ kΩ. We want to note that $Z_L/n \propto A^{3/2}V_{RF}^{1/4}$ and $Z_{sh}/Q \propto AV_{RF}^{1/2}$, where A is the bunch area. Thus, if the bunch area is reduced to 0.1 eV-sec, these limits will become 2.33 Ω and 10.7 kΩ respectively. Sometimes, 3 batches are accelerated but each batch has to be extracted only every one or two seconds so that the lithium lens will not be heated up by too much. Under this situation, during the extraction of the first batch, the 4 MV RF is turned on for about 2.5 ms or half a synchrotron period only so that the bunches that are not extracted will rotate to the position of maximum time spread. The process is now reverse by lowering the RF to 300 kV to allow the bunches to rotate for a quarter synchrotron oscillation and increasing it abruptly to 4 MV again. The bunches now match the 4 MV buckets. The whole process is repeated again when the next batch is ready for extraction. In this way, the bunches will stay in the most dangerous position of maximum time spread for a quarter of a synchrotron oscillation only. If there is a microwave instability, the microwave amplitude will not have enough time to grow appreciably.

12.3 Longitudinal Impedance Estimation

Single bunch microwave instabilities are driven by impedances at high frequencies, single bunch mode-coupling instabilities are driven by impedances at low frequencies, and coupled-bunch instabilities are driven by resonances with high quality factors. Thus we need to estimate impedances of the Main Ring at both low and high frequencies[12.3.1].

Resistive wall

For a circular beam pipe of length ℓ, radius b, and conductivity σ, the electromagnetic field of the beam will penetrate into the wall of the pipe by a skin depth $\delta = (2/\mu\omega\sigma)^{1/2}$, where μ is the permeability of the pipe material and $\omega/2\pi$ the frequency of the electromagnetic wave. Thus, the beam will see an impedance due to a strip of pipe material of length ℓ, width 2πb, and thickness δ. In other words,

$$Z_L = (1+j)\ell/(2\pi b\delta\sigma). \qquad (12.3.1)$$

The inductive part comes about because the electromagnetic wave flowing into the surface of the beam pipe has to attenuate by a factor of 1/e after penetrating a distance δ, and, therefore, the wave number contains an imaginary part.

For a rectangular beam pipe of width w and height h, the return current of the beam does not distribute uniformly on the walls. Thus, the longitudinal wall impedance cannot be derived so simply as the circular beam pipe. However, a detailed derivation gives an expression[12.3.2] very similar to Eq. (12.3.1),

$$Z_L = (1+j)F_L \ell/(\pi h \delta \sigma). \qquad (12.3.2)$$

Here, h/2 takes the place of the radius b and a form factor F_L takes care of the fact the pipe is rectangular in cross section.

The vacuum chamber of the Main Ring consists of beam pipes of different cross sections: 8136 ft of 1.5"x5" and 8496 ft of 2"x4" rectangular beam pipes inside the dipoles and parts of the straight sections, 1536 ft of rhomic pipes (approximate circular radius 3.8 cm) for the quads, 624 ft of 6" circular pipes in part of the straight sections, and 188.75 ft of 5" circular pipe in the RF region. The pipe in the RF region is of copper while the rest is of stainless steel. The form factors F_L for the 1.5"x5" and 2"x4" pipes are taken as unity[12.3.2] with an error less than 2.5%. The rhomic pipes are approximated by circular pipes of radius 3.8 cm. Assuming a conductivity of $\sigma = 0.14\times10^7$ mho-m^{-1} for stainless steel and 5.8×10^7 mho-m^{-1} for copper, the total contributions to the wall impedance is

$$Z_L/n = (1+j)14.5n^{-1/2}\ \Omega, \qquad (12.3.3)$$

where n is the revolution harmonic of the frequency of the electromagnetic wave under consideration. Comparing with the limits obtained in the previous section, we see that the wall impedance is too small to drive a fast instability in the microwave region, which is usually taken as $n = R/b$, where R is the mean radius of the Main Ring and b is the mean radius of the vacuum chamber.

Bellows

The Main Ring bellow housings serve the purpose of joining beam pipes together and provide some leeways in both the horizontal and vertical directions. A typical bellow consists of a pill-box cavity of length g ~ 15.85 cm and radius d ~ 7.16 cm with only four to five ripples at one end and a porthole connected to the vacuum pump. Because of the smallness of the ripple width and depth compared with the dimension of the pill box, the electromagnetic fields hardly go into the ripples. In other words, the main contribution to the bellow impedance comes from the pill box itself: the steps between the pill box and the side-pipes at low frequencies and the resonances of the pill box at high frequencies.

When a particle passes through the pill box, electromagnetic fields are left and trapped inside the pill box. However, at low frequencies, only magnetic flux can be trapped because electric field cannot satisfy the boundary conditions, (Fig. 12.3.1a). These trapped magnetic flux ϕ_t will induce a back e.m.f.

$$\int E_z dz = -j\omega\phi_t \qquad (12.3.4)$$

on the beam itself. If the length of the cavity g is less than or of the same order as the steps 2(d-b), the amount of trapped flux is

$$\phi_o = g(\mu_o I_\omega/2\pi)\ell n(d/b), \qquad (12.3.5)$$

where b = 3.61 cm is the radius of the side-pipes, I_ω the components of the longitudinal current wave with frequency ω, and μ_o the permeability of free space. The longitudinal impedance per harmonic seen the the beam at frequency ω is therefore

$$Z_L = jZ_o(\beta g/2\pi R)\ell n(d/b), \qquad (12.3.6)$$

where Z_o = 377 Ω, βc the phase velocity of the current wave, and R = 1 km the mean radius of the Main Ring. Equation (12.3.6) was first derived by Keil and Zotter by solving some complicated matrix equations[12.3.3].

When g >> 2(d-b) which is our case, only the flux near the corners will be trapped and that in the middle will leak away (Fig. 12.3.1b). Thus, g in Eqs. (12.3.5) and (12.3.6) should be replaced by ~2(d-b). We therefore obtain the impedance per harmonic $Z_L/n \sim j2.9$ Ω for ~1000 bellow housings at low frequencies ($n<<g/2\pi R$). A numerical computation using the code[12.3.3] TBCI yields $Z_L/n = j2.4$ Ω.

At high frequencies, in order to study the resonances of the pill box, we make the approximation that the pill box is closed (no side-pipes) and neglect the ripples and the porthole. The impedance can then be computed exactly. The first few modes that contribute to the longitudinal impedance are the TM_{01p} modes. The longitudinal electric fields are proportional to

$$\epsilon_p(r,z,t) = J_o(x_1 r/d)\cos(p\pi z/g)\exp(j\omega_p t), \qquad (12.3.7)$$

where J_o is the Bessel function of order zero and x_1 = 2.405 is its first zero. The resonance frequency $\omega_p/2\pi$ is given by

$$(\omega_p/c)^2 = (x_1/d)^2 + (p\pi/g)^2. \qquad (12.3.8)$$

The 4 lowest modes therefore have frequencies 1.60, 1.92, 2.48 and 3.26 GHz. The higher modes need not be considered because they are above the cutoff frequency ~3.2 GHz of the beam pipes. The fields of these modes will no longer be trapped inside the pill box. They will propagate away along the beam pipes and therefore will not contribute to the impedance significantly.

The resonance modes are excited by a beam particle passing through the pill box along the central axis. The amount of excitation for a certain mode will therefore be proportional to

$$\int_0^g \epsilon_p^*(0,z,t)dz, \qquad (12.3.9)$$

where ϵ_p is given by Eq. (12.3.7). In the above integration, $t = (z-z_o)/\beta c$ is considered a function of z. It denotes the time when the particle travelling at velocity βc is at a certain location inside the pill box; for example, $t = 0$ when $z = z_o$. The total retarding force seen by the particle traversing the pill box is proportional to ϕ_p^*. The shunt impedance per quality factor of the resonance Z_{sh}/Q is given by

$$(Z_{sh}/Q)_p = Z_o|\phi|^2 C_p/(\omega_p/c), \tag{12.3.10}$$

where $Z_o = 377\ \Omega$, and C_p is a normalization constant defined as

$$C_p \int |\vec{\epsilon}_p|^2 2\pi r dr dz = 1. \tag{12.3.11}$$

Equation (12.3.10) then becomes

$$(Z_{sh}/Q)_p = Z_o(c/\omega_p d)(g/d)|\phi/g|^2 a_p/[\pi J_1^2(x_1)], \tag{12.3.12}$$

where J_1 is the Bessel function of order 1 and $a_p = 1.00, 1.48, 0.84, 0.48$ for $p = 1, 2, 3, 4$.

The results for the first four modes are listed in Table 12.3.1 and the electric field configurations are displayed in Fig. 12.3.2. We see that Z_{sh}/Q for the first mode is very much smaller than the rest. This is because the longitudinal electric field is constant along the pill-box axis. But at a resonance frequency of 1.60 GHz, this field changes sign as the particle reaches the middle of the pill box. Therefore, the total retarding force seen by the particle is nearly zero. On the other hand, the longitudinal electric field for the second mode behaves like $\cos(\pi z/g)$, or it is of opposite signs for the two halves of the pill box as depicted in Fig. 12.3.2. At a resonance frequency of 1.92 GHz, the electric field also changes sign as the particle reaches the middle of the box. But, in this case, the particle will be seeing retarding force of one sign only and the impedance becomes enhanced. This effect is known as the transit-time effect and the information is contained in the transit-time factor $T = |\phi/g|^2$ which is listed in Table 12.3.1 also.

For open-end pill box, numerical computation is required. We try to run the code[12.3.3] TBCI by assuming that the beam pipes on both sides are circular and are of radius ~3.61 cm, which corresponds to a cutoff frequency of ~3.2 GHz. The Fourier transform of the wake field shows 4 resonances at roughly the positions predicted above (Fig. 12.3.3). The addition of the bellow ripples does not change the result appreciably. We next analyze the pill box with closed side pipes in the frequency domain using the code[12.3.4] URMEL, from which the quality factors Q and Z_{sh}/Q for the first four modes are obtained. These numerical results are also listed in Table 12.3.1 for comparison. We note that these results do not differ from those of the closed pill box by very much except for the Z_{sh}/Q of the first mode. However, the

impedance of the first mode is very sensitive to the transit-time effect because of the near cancellation. Thus, it is not unexpected that the impedance will change by very much when the side pipes are added.

The Main Ring has about 1000 such bellow systems; the radii and lengths have standard deviations $\Delta d/d = 0.003$ and $\Delta g/g = 0.034$. Thus, the frequency of resonance will have a spread and the resonance will be broadened. However, the quality factor of one bellow pill box is of the order $Q \sim 2V/S\delta \sim 4500$, where V and S are the volume and the internal surface area of the pill box and δ is the skin depth. The broadened resonances are still very much narrower than the width of the spectrum of a bunch. As a result, Z_{sh}/Q should be quoted instead of Z_L/n. Using the numerical results, for 1000 bellow systems, Z_{sh}/Q = 2.4, 37.0, 24.3, and 28.9 kΩ for the four resonances. From Table 12.2.1, the stability limit for proton-bunch coalescence is only $Z_{sh}/Q = 9.5$ kΩ. Therefore, these resonances will definitely drive microwave instabilities during bunch coalescence. During the shutdown of the Main Ring from 1985 to 1986, sleeve pieces with tapered ends are installed inside the bellow pill boxes so that a bunch will see a smooth transition from one beam pipe to another. As is verified by the wire measurement experiment discussed later in Section 12.4, the four resonances will be completely shielded off and the bellow systems will no longer contribute significantly to the impedance of the machine.

Beam Position Monitors

There are about M = 216 beam position monitors in the Main Ring. They are rectangular in shape, $\ell = 11.75$ cm in length, slant cut diagonally and terminated at the center by a resistance of 25 ohms. A typical horizontal monitor is shown in Fig. 12.3.4a. We try to approximate it by two half-cylindrical strip plates each with an open angle $\phi_o = \pi$. Each plate can then be viewed as a transmission line with respect to the beam pipe, (Fig. 12.3.4b). The characteristic impedance Z_c is taken as 25 ohms also. At very low longitudinal frequency ω, the input impedance Z_i seen at one end of the plate is nearly Z_c and therefore there will not be any reflection. If we keep the lowest reactive term,

$$Z_i = Z_c(1-j\omega\ell/2c). \tag{12.3.13}$$

For a beam current of the form $I(t) = I_\omega e^{j\omega t}$ where ω is small or more precisely $\omega\ell/c \ll 1$, the image current sees a voltage V_u at the upstream end and a voltage V_d at the downstream end. They are

$$V_u = Z_i(\phi_o/2\pi)I(t), \tag{12.3.14}$$

$$V_d = -Z_i(\phi_o/2\pi)I(t-\ell/\beta c), \tag{12.3.15}$$

where βc is the phase velocity of the beam current. The voltage seen by the beam is therefore

$$V = (\phi_o/2\pi)(V_u - V_d), \tag{12.3.16}$$

or

$$V = Z_i(\phi_o/2\pi)^2[I(t) - I(t-\ell/\beta c)]. \tag{12.3.17}$$

The extra factor of $\phi_o/2\pi$ comes about because the interaction on the beam comes from the plate which surrounds only $\phi_o/2\pi$ of the beam. Putting in Z_i and $I(t)$, we get

$$V = Z_c I_\omega(\phi_o/2\pi)^2(1-j\omega\ell/c)[1-e^{-j\omega\ell/\beta c}]. \tag{12.3.18}$$

Thus, for one plate, the impedance seen by the beam at low frequencies is $Z_L = V/I_\omega$, or

$$Z_L = Z_c(\phi_o/2\pi)^2(\omega\ell/\beta c)(j+\omega\ell/c). \tag{12.3.19}$$

The total impedance for 216 monitors or 432 plates is therefore

$$Z_L/n = (j0.317 + 3.73\times10^{-5}n) \text{ ohms}. \tag{12.3.20}$$

At high frequencies, the plate can accept resonances with the standing waves having a node at the middle because the termination impedance there does not absorb any power and the resonances will not be disturbed. In other words, the possible resonating wavelength is

$$\lambda_m = m\ell/2, \tag{12.3.21}$$

where $m = 1, 3, 5, \ldots$ This relationship can also be obtained by equating the input impedance

$$Z_i = jZ_c\cot(\omega\ell/c) \tag{12.3.22}$$

of the open-ended transmission line to infinity. To compute the shunt impedance, we include a small surface impedance per unit length

$$R = 1/(\phi_o b\delta\sigma), \tag{12.3.23}$$

where b is the radius of the cylindrical monitor plate, σ the conductivity and δ the skin depth. Then, in Eq. (12.3.22), $1/c$, which is equal to $(LC)^{1/2}$ where L and C are the inductance and capacitance per unit length of the plate, should be replaced by

$$1/c = \{[L + (1+j)R/j\omega]C\}^{1/2}. \tag{12.3.24}$$

Assuming that $R\ell << Z_c = (L/C)^{1/2}$, Eq. (12.3.22) is expanded in the vicinity of the resonance frequency $\omega_m = m\pi c/\ell$ to become

$$Z_i \sim \frac{2Z_c^2/R}{1 + j(2m\pi Z_c/R\ell)(\omega/\omega_m - 1)}, \tag{12.3.25}$$

We can then read off the shunt impedance Z_{sh} and the quality factor Q,

$$Z_{sh} = 2Z_c^2/R \ , \quad Q = m\pi Z_c/R \ , \tag{12.3.26}$$

or

$$Z_{sh}/Q = 2Z_c/m\pi. \tag{12.3.27}$$

It is interesting to point out that Z_{sh}/Q, as given in Eq. (12.3.27), depends only on the characteristic impedance of the plate and is independent of its actual shape provided that the plate is terminated at the middle by an impedance equal to Z_c. The results for the first four modes are listed in Table 12.3.2. We see that the contribution of the first mode is the largest; Z_{sh}/Q = 6.9 kΩ for 216 monitor systems or 432 monitor plates. Although the most stringent limit for the Main Ring is Z_{sh}/Q = 9.5 kΩ, the crudeness of our estimation tells us that this mode should be considered dangerous.

Kickers

The Main Ring contains extraction kickers for transferring protons and antiprotons to the Energy-Saver and protons for antiproton-production, abort kicker for protons, and also injection kickers for transferring protons from the booster and antiprotons from the accumulator. These kickers are of the form of window-frame magnets either of size 2" × 6" and length ℓ = 1 m or 1 1/2" × 3 3/8" and length ℓ = 1.9 m. If the beam passes through the center of the magnet, the magnetic flux it links inside the magnet just is equal the return flux it links outside the magnet. In other words, there will not be any voltage induced on the beam by the magnet. If the beam deviates from the central axis by x_o, the flux it links is (Fig. 12.3.5)

$$\phi = \mu_o I_k (x_o \ell/h), \tag{12.3.28}$$

where h is the height of the magnet whose width is w, I_k the current in the magnet windings, and μ_o the permeability of free space. Therefore, there is a mutual inductance of $M = \mu_o x_o \ell/h$ between the horizontally deviated beam and the kicker current. Thus, the beam current I_b induces a voltage $V_k = jwM$ in the magnet windings, which in turn induce a back e.m.f. $jwMV_k/Z_k$ on the beam. The impedance seen by the beam is therefore $Z_L = -\omega_o^2 M^2/Z_k$. Here, $Z_k = j\omega L + Z_g$ is the impedance of the magnetic circuit; the first term is the generator impedance including cables while the second term with the inductance equal to $\mu_o w/h$ is the impedance due to the magnetic fields it produces. If one neglects Z_g one gets[12.3.5]

$$Z_L/n = Z_o x_o^2 \ell/RA_m, \tag{12.3.29}$$

where Z_o = 377 Ω, A_m = w×h the cross sectional area of the window-frame magnet, and R the mean radius of the Main Ring.

Taking the horizontal dispersion function $\eta \sim 5$ m and $\sqrt{6}\sigma_p/p \sim 10^{-3}$, the deviation of the beam is $x_o \sim 1$ mm. However, at injection, the beam has a 95% betatron emittance of 2.5 mm-mr or a transverse spread of ~1.58 cm. Taking the latter as x_o, we obtain for the Main Ring kickers at low frequencies $Z_L/n = 0.03\ \Omega$, which will be to small for instability.

Lambertsons

Lambertson magnets are required for the injection and extraction of the particle beam. The cross section of a typical Lambertson is shown in Fig. 12.3.6a. The beam will see laminations of thickness $\tau \sim 0.953$ cm separated by gaps or cracks $\Delta \sim 28.6\ \mu$m. There are two Lambertsons each of length 120" at E0, two Lambertson each of length 204" at F0, one Lambertson of length 90" at A0 and two Lambertson each of length 181" at C0. In total, the Lambertsons occupy a length of $L = 1016$"; or there are roughly $N \sim 2.71\times10^4$ laminations. The laminations are approximated as annular rings of inner and outer radii b = 1" and b+d = 2" respectively and are shorted at the outer end as shown in Fig. 12.3.6b. The relative magnetic permeability and the conductivity of the lamination are taken as $\mu_L \sim 100$ and $\sigma_L \sim 0.5\times10^7$ mho/m respectively. The dielectric constant and conductivity of the material filling the cracks are taken as $\epsilon_1 \sim 6$ and $\sigma_1 \sim 0.01$ mho/m respectively.

Each crack can be viewed as a transmission line. The impedance seen by the beam is contributed by the image current flowing around each lamination and also field penetrating into the cracks. At frequencies, $f << \mu_L c/(\pi\sigma\Delta^2 Z_o)$ or ~6 GHz, the former contribution dominates. Similar to the resistive wall derivation, the longitudinal impedance is

$$Z_L = (1+j)N\ell n(1+d/b)/(\pi\delta\sigma), \qquad (12.3.30)$$

where δ is the skin depth in a lamination. This amounts to $Z_L/n = (1+j)11.6n^{-1/2}\ \Omega$.

If we further approximate the crack to be a parallel plate transmission line of width $2\pi b$, the first resonance can be estimated. The impedance per unit length along the lamination is $z = (1+j)/(\pi\delta\sigma)$ while the admittance per unit length is $y = j\omega\epsilon_o\epsilon_1\Delta/2\pi b$ where ϵ_o is the permittivity of free space and the conductivity of the medium has been neglected. The wave going into the crack has the propagating constant $\gamma = (yz)^{1/2}$. The first resonance is roughly given by $Im(2\gamma d) = \pi$. Putting in the data, we obtain $\gamma d = (1.11+j2.69)f^{3/4}$, where the frequency $f = \omega/2\pi$ is in GHz. The characteristic impedance is $Z_c = (z/y)^{1/2} = 0.0615e^{j3\pi/8}f^{1/4}$. Thus, the first resonance is at 0.488 GHz where $|Z_c| = 0.0736\ \Omega$. The impedance seen by the beam is $Z_i = Z_c\tanh(\gamma d)$. An estimate of $\tanh(\gamma d)$ at resonance is $(1+e^{-2\alpha})/(1-e^{-2\alpha})$ or 1.74, where $\alpha = Re(\gamma d)$. Therefore, for all $N \sim 2.71\times10^4$ laminations, the shunt impedance is $Z_{sh} = 3470\ \Omega$. The quality factor is $Q \sim \Delta/2\delta$ or ~14. An actual numerical computation gives the first

resonance at 0.47 GHz with shunt impedance 3460 Ω. The wall impedance increases with frequency; so we expect the higher resonances to be damped heavily and will appear as ripples only. This is verified by the numerically computed impedance shown in Fig.12.3.7.

Summary

The contributions to the longitudinal impedance estimated in above are plotted in Fig. 12.3.8 and listed in Table 12.3.3. We see that near cutoff frequency, the most important contributions come from the bellow housings and the beam monitors. They are big enough to drive microwave instabilities. If sleeves are installed inside the bellows to smooth out the steps and shield off the pill-box structure, all the bellow contribution will vanish. In that case, the beam monitors will become the most dangerous threat to stability.

12.4 Wire Measurement Experiment

A wire carrying a current is placed inside a beam pipe to simulate the effect due to a particle beam. The potential difference across the wire will give a measure of the impedance due to the discontinuities of the beam pipe. Such an experiment had been carried out by J. Reid[12.4.1].

Experimental Setup

Four sections of the Main Ring beam pipe about 26" long with flanges were configured to simulate different devices. Pipe A is the standard 2"x4" rectangular beam pipe with flanges at each end and was used as the reference (Figs. 12.4.1a and 12.4.1b). Pipe B is a Main Ring bellow system inside the same beam pipe as A (Fig. 12.4.1c) and Pipe C consists of exactly the same bellows as B but with sleeve pieces inside connecting the side pipes and shielding the bellow ripples and pill-box structure. Pipe D contains a Main Ring bellow system which includes a beam monitor (Fig. 12.4.1d); the detector can be vertical or horizontal and the system can be assembled with or without sleeve pieces.

A wire of 1/16" diameter was strung down the center of the standard pipe. The characteristic impedance of this wire in the rectangular beam pipe is approximately $Z_c \sim 216\ \Omega$. To match this characteristic impedance to the 50 Ω RG58 cables on each side, a minimum loss L-pad matching network was installed on each side as in Fig. 12.4.2a. In order that signals coming out of the beam pipe see 216 Ω, we need

$$1/(1/Z_2+1/50) + Z_1 = 216. \qquad (12.4.1)$$

In order that signals from the RG58 cable entering the beam pipe to see 50 Ω, we need

$$1/(Z_1+216) + 1/Z_2 = 1/50. \qquad (12.4.2)$$

These give $Z_1 = 189.357\ \Omega$ and $Z_2 = 57.035\ \Omega$. The actual best match was accomplished by choosing $Z_1 = 191\ \Omega$ and $Z_2 = 57\ \Omega$. This match is ex-

tremely important because we do not want any reflection from each connection between the beam pipe and the RG57 cable, so that the whole system with the standard pipe A will not introduce any voltage drop except at the L-pads which can be computed. At the input end, the attenuation is

$$a_i = 216/(Z_1 + 216), \tag{12.4.3}$$

which is 0.4693 or -5.502 db. At the output end, the attenuation is

$$a_o = Z_3/(Z_1 + Z_3), \tag{12.4.4}$$

where Z_3 is Z_2 and 50 Ω in parallel. Therefore, a_o = 0.1224 or -18.178 db. Thus, a signal passing through the system will show an attenuation of -23.68 db. If there is a discontinuity in the beam pipe, for example, a bellow housing or a beam monitor, contributing an impedance Z, a signal with a voltage E_1 entering the beam pipe will be reflected at the discontinuity with a reflection coefficient

$$\rho = \frac{(Z_c+Z) - Z_c}{(Z_c+Z) + Z_c}, \tag{12.4.5}$$

so that the voltage at the beginning of the discontinuity is $E_2 = (1+\rho)E_1$. Then, the voltage at the end of the discontinuity is, from Fig. 12.4.2b, $E_3 = E_2Z_c/(Z_c+Z)$. The additional attenuation is defined as $a = E_3/E_1$. Therefore,

$$a = 2Z_c/(2Z_c+Z), \tag{12.4.6}$$

or the impedance of the discontinuity is

$$Z = 2Z_c(1-a)/a. \tag{12.4.7}$$

Two different network analyzers were employed. An HP model 8754A was used for frequencies up to 1.36 GHz, while to frequencies up to 3.56 GHz, a modified version of the HP 8410 automatic network analyzer with HP accuracy enhancement pac was used.

The results of the test pipe calibration is shown in Fig. 12.4.3. The results show how well the impedance matching was. At high frequencies, the calibration curve exhibits some variations. This is in fact expected. The resistors used in the L-pads are of the 1/4 watt Allen Bradley type. At high frequencies, they are not just pure resistors anymore and therefore the matching will not be exact. Figure 12.4.3 also defines the resolution of the setup, which was approximately 1.5 db corresponding to ~81 Ω. Since the purpose of this measurement was to look for large impedances, such a resolution was acceptable.

Results of Measurement

Replacing the reference pipe with Pipe B containing the Main Ring bellow housing, the results are shown in Fig. 12.4.4a and Table 12.4.1. We see that the results agree with the predicted estimates in Section 12.3, which are also listed alongside for comparison. The only resonance that does not agree is the fourth one. But the experimental setup was not designed to give consistent large impedance magnitudes in the upper frequency range. This is due to the ill-behavior of the Allen Bradley resistors and also in part due to the mechanical placement of the wire and associated pieces of the beam pipe.

We need to point out that a wire inside a beam pipe can support TEM mode which has no cutoff frequency. In other words, any resonance fields inside the bellow housing can leak away along the beam pipe although the frequency is below the TM-mode cutoff frequency of the beam pipe. As a result, the quality factors measured here will be very small and they have nothing to do with the quality factors of the resonances excited by an actual particle beam which does not support any TEM mode. As a result, the measured shunt impedances will be very much smaller also. The only meaningful quantities to look at may be Z_{sh}/Q.

Using Pipe C with sleeve pieces shielding the bellow ripples and the pill-box discontinuity, the results are shown in Fig. 12.4.4b. Here, there are no measurable modes up to 3.5 GHz.

Pipe D containing the Main Ring horizontal beam detector assembly was first measured with no sleeve. Figure 12.4.5a and Table 12.4.2a show the results. We see that the lowest resonance mode is at 794 MHz, very much lower than the estimated 1.2 GHz. This may be because the estimation was made assuming two straight cylindrical strips of length 11.75 cm. The actual beam monitor is diagonally cut (Fig. 12.3.4a) with a cut length of ~15.53 cm. Together with some end effects, this may be able to support a mode of much lower frequency than 1.2 GHz. Thus, the former estimates may have been too crude for comparison here. On the other hand, the lowering of the resonance frequency may be due to the geometry of the experimental setup and the presence of the wire instead of a beam. From Table 12.4.2a, we see that Z_{sh}/Q decreases roughly like 1/m for m = 1, 3, 5, ... In any case, for 216 monitors, a Z_{sh}/Q = 4.5 kΩ or 9.7 kΩ is definitely too large for the stability of the beam.

With sleeve pieces installed, the measurements of the horizontal beam monitor are shown in Fig. 12.4.5b and Table 12.4.2b. The lowest and most dangerous mode at ~800 MHz appears to have been damped, but the second mode is not and is therefore still a threat to stability. The mode at 2.1 GHz disappears.

Conclusions

The addition of the sleeves inside the Main Ring bellows is dramatic. It eliminates all measurable modes up to 3.5 GHz. The addition

of sleeves in the beam monitor is less dramatic. Although the ~800 MHz mode is suppressed and the 2.1 GHz mode is eliminated, the 1.6 GHz mode is still a threat to stability.

We need also to keep in mind that a wire inside a beam pipe is nevertheless different from an actual particle beam. For example, with the wire there is a continuum of TEM modes which are certainly not present when the wire is replaced by a particle beam. As a result, the results of a wire-measurement experiment can only be considered as a guide or reference.

12.5 Measurement of Impedance by Debunching

When the RF voltage is turned off suddenly, the once bucket-matched bunch will start to shear because particles with different energies travel with different angular velocities. The bunch becomes longer and longer while the energy spread becomes smaller and smaller with the bunch area unchanged. According to the microwave stability criteria, Eqs. (12.1.10) and (12.1.13), the critical $Z_L/n \propto \sigma_E$ if the driving impedance is a broad band and the critical $Z_{sh}/Q \propto \sigma_E^2$ if the driving impedance is a narrow resonance. Thus, a time will reach when the bunch becomes unstable. From the microwave signals measured during the growth, we can determine the longitudinal impedance in the ring that drives the instability[12.5.1].

Such an experiment was carried out by Jim Crisp[12.5.2] for the Main Ring.

The Experiment

Nine bunches each of intensity $N = 0.636 \times 10^{10}$ protons were accelerated to 150 GeV and were left in buckets with RF voltage equal to $V_{RF} = 1.079$ MV. The RF voltage was turned off suddenly and the bunches tended to shear. When the energy spread is small enough, Landau damping failed and microwave signals started to grow.

A coaxial directional coupler designed by Jim Griffin[12.5.3] was used to pick up the microwave signals. The detector consists of two concentric pipes a quarter wavelength long having a characteristic impedance of 12.5 Ω. Each end has four symmetrically spaced 50 Ω ports. The signals were transported from the enclosure via a 177 nsec long 7/8" heliax cable. A spectrum analyzer in the zero-span mode was used to monitor the amplitude of the 31st harmonic of the RF ($f_{MW} = 1.646$ GHz). Zero-span mode basically plots the amplitude of the signal that passes through an equivalent filter with the center frequency and bandwidth specified. The peak detector was not used because it has the disadvantage that the signal must overcome the diode forward voltage drop before it can be detected, whereas the spectrum analyzer has a linear response to small signals and a logarithmic scale. The photos in Fig. 12.5.1 compare the displays of the spectrum analyzer and peak detector for a typical run. The diode detector indicates a time of 60 msec for the onset of the microwave growth but the analyzer shows a clear minimum at about 30 msec.

Theory

The original bunch has RMS time spread and energy spread $\hat{\sigma}_\tau$ and $\hat{\sigma}_E$ respectively. After time t, they become σ_τ and σ_E respectively. Any particle with an energy ΔE bigger than the synchronous particle will be ahead of it by an extra time

$$\Delta\tau \sim \eta t(\Delta E/E), \tag{12.5.1}$$

where η is the frequency dispersion (or frequency slip) parameter. A particle at the RMS bunch width σ_τ will come from the center of the original bunch with an excess energy equal to $\hat{\sigma}_E$, or

$$\sigma_\tau \sim \eta t\hat{\sigma}_E/E. \tag{12.5.2}$$

Remembering that $\sigma_\tau\sigma_E$ being proportional to the bunch area is equal to $\hat{\sigma}_\tau\hat{\sigma}_E$, the stability criteria of Eqs. (12.1.10) and (12.1.13) become

$$\left(\frac{Z_L}{n}\right)t_o = \frac{(2\pi)^{3/2}\hat{\sigma}_\tau^2(\hat{\sigma}_E/e)}{eN}, \tag{12.5.3}$$

and

$$\left(\frac{Z_{sh}}{Q}\right)t_o^2 = \frac{4\hat{\sigma}_\tau^2(E/e)}{\eta I_{AV}}. \tag{12.5.4}$$

where N is the number of particles in a bunch with average current I_{AV} and t_o is the time when instability starts. Thus, knowing t_o, the magnitude of the driving impedance can be computed.

Results Analysis

1. Bunch shape

The stability criteria used in the above are for a Gaussian bunch only. Thus, one should check whether our bunches are Gaussian or not. A typical bunch shape is selected and is fitted by a Gaussian curve with RMS time spread $\hat{\sigma}_\tau$ and also a parabolic curve with maximum half spread $\hat{\tau}$. The results are shown in Fig. 12.5.2 The normalized sum of deviation of the Gaussian fit is about ten times less than that of the parabolic fit. So we accept the bunch to be Gaussian. The best RMS time spread obtained is $\hat{\sigma}_\tau$ = 0.635 cm. The RF voltage was 1.074 MV. This leads to a RMS energy spread of $\hat{\sigma}_E$ = 0.0192 GeV and a bunch area of $6\pi\hat{\sigma}_\tau\hat{\sigma}_E$ = 0.230 eV-sec.

2. Starting time of growth

As seen in the stability criteria of Eqs. (12.5.3) and (12.5.4), the starting time of growth t_o is very crucial to the determination of the driving impedance. From Fig. 12.5.1 it is clear that the bunch is unstable at 30 msec, but the actual growth may have started before that.

In order to determine t_o more accurately, the growth rate is computed as a function of time from a dispersion relation[12.5.3]. At time $t = t_o(1+x)$, the logarithmic power growth is proportional to the function $F(x)$, which is plotted in Fig. 12.5.3 By comparing the maximum slope at $x = 2.25$ and the change in slope from $x = 0$ to 2.25 with the actual logarithmic growth measured in Fig. 12.5.1 we conclude that the starting time of growth is $t_o \sim 20$ msec.

3. Overlapped bunches

Two adjacent bunches start to touch each other when the half bunch length $\sqrt{6}\sigma_\tau$ is equal to the half length of a bucket $\pi/h\omega_o$, where h is the RF harmonic and $\omega_o/2\pi$ is the revolution frequency. Putting this into the left side of Eq. (12.5.1) and letting ΔE equal to the half energy spread of the bunch $\sqrt{6}\delta_E$, the time when two adjacent bunches touch each other is

$$t = \pi/[\eta h\omega_o(\sqrt{6}\delta_E/E)], \qquad (12.5.5)$$

which gives 9.3 msec. Thus, when instability starts at ~20 msec, two adjacent bunches overlap completely. We are faced with two questions. Which energy spread should we used in the stability criteria? If we use the actual energy difference between the two bunches other than the energy spread σ_E of one bunch, the bunch will be much more stable, (Fig. 12.5.4). Should we take the sum of the currents of the two bunches as the current in the criteria; the bunch will then be less stable.

This problem can be solved[12.5.4] by examining two coasting beams one with revolution angular frequency ω_1 and the other ω_2 and each has a RMS angular frequency spread of σ_ω. We also assume that $\sigma_\omega \ll \Delta\omega$ where $\Delta\omega = |\omega_1-\omega_2|$. Imagine a small perturbing longitudinal current wave of the form $I_1 e^{j(\Omega t-n\theta)}$ where θ is the azimuthal angle around the accelerator ring. If the coherent frequency $\Omega \sim n\omega_1$, it will set the particles in the first beam to oscillate with harmonic n and eventually lead to a growth if the frequency spread σ_ω is not big enough to destroy the coherency. Since $\sigma_\omega \ll \Delta\omega$, the particles in the second beam will not be affected. On the other hand, if the coherent frequency of the perturbation is $\Omega \sim n\omega_2$, it can only drive a growth of harmonic n in the second beam while the first one is not affected. Thus, the stability criterion is for one beam only; i.e., it involves σ_ω or σ_E instead of $\Delta\omega$ or ΔE, and the current is the local current of one bunch only. In other word, the stability criterion remains unchanged; it is exactly that for one bunch. An actual solution of the Vlasov equation for two overlapped bunches give a stability curve that wraps around the origin of the $(\Delta\Omega/n)^2$-plane two times as in Fig. 12.5.5, where the stability curve for one bunch is also shown for comparison. Take the situation when the driving impedance is capacitive and above transition. The stability point for one bunch is the point A. For two bunches, there are two such points A_1 and A_2, where the stability curve

crosses the negative imaginary $(\Delta\Omega/n)^2$-axis twice. In fact, these two points coincide each other and are very close to the point A if $\sigma_\omega << \Delta\omega$. Note that the points A_1 and A_2 correspond to very different coherent frequencies Ω, the different being $n\Delta\omega$.

4. Determination of driving impedance

Having the correct stability criterion and knowing the starting time of growth, the driving impedance can now be computed. Here, we assume that the driving impedance is the peak of a broad band or a narrow resonance; or it is real. Therefore, it corresponds to the points B_1 or B_2 on the stability curve of Fig. 12.5.5 and are about 1.434 times (for Gaussian beam only) farther away from the origin than the points A_1 or A_2, for which the stability criteria of Eqs. (12.5.3) and (12.5.4) are derived. When this factor of 1.434 is included, we obtain at 1.64 GHz, $Z_L/n = 8.6\ \Omega$ for a broad band and $Z_{sh}/Q = 6.4\ k\Omega$ for a narrow resonance. In the impedance estimation of Section 12.3, there is not any broad-band impedance around 1.64 GHz. Therefore, the driving force may come from sharp resonances. Possible candidates are the first resonance of the beam monitors with $Z_{sh}/Q = 6.9\ k\Omega$ at ~1.28 GHz and the second bellow-housing resonance with $Z_{sh}/Q = 2.4\ k\Omega$ at ~1.6 GHz.

We want to point out that, since the starting time of growth t_o is not evident from Fig. 12.5.1, its theoretical determination in above is not without controversy. Any change in t_o will affect the final results for the driving impedance. For this reason, the computed results may include some big inaccuracy.

REFERENCES

12.1.1 A. Hofmann, Proceedings of the First Course of the International School of Particle Accelerators of the 'Ettore Majorana' Center for Scientific Culture, Erice, 1977, p.139.

12.1.2 E. Keil and W. Schnell, CERN Report ISR-TH-RF/69-48 (1969).

12.1.3 S. Krinsky and J. M. Wang, Particle Accelerators **17**, 109 (1985).

12.1.4 If we include only the real part of the resonance and let Q tend to infinity, this criterion can be obtained easily. However, the neglect of the imaginary part which carries a long tail is a violation of causality.

12.2.1 K. Y. Ng, Fermilab Report TM-1383.

12.2.2 S. Y. Lee and J. M. Wang, IEEE Transaction on Nuclear Science **NS 32**, 2323 (1985).

12.3.1 K. Y. Ng, Fermilab Report TM-1388.

12.3.2 K. Y. Ng, Particle Accelerators **16**, 63 (1984).

12.3.3 T. Weiland, DESY 82-015, 1982.

12.3.4 T. Weiland, DESY M-82-24, 1982.

12.3.5 G Nassibian and F. Sacherer, CERN/ISR-TH/77-61.

12.4.1 J. Reid, Fermilab Internal Report.

12.5.1 K. Y. Ng, Fermilab Report TM-1389.

12.5.2 J. Crisp, Fermilab Internal Report.

12.5.3 B. A. Prichard, J. E. Griffin, R. F. Stiening and E. Wilson, Fermilab EXP. 74, 1975.

12.5.4 K. Y. Ng, Proceedings of the Second Conference on the Intersection between Particle and Nuclear Physics, Lake Louise, May 26-31, 1986, p. 401.

Table 12.2.1 Coalescence of 7 proton bunches at 150 GeV

	Start	V_{RF} lowered to match bunch	7 bunches in h=53 bucket	End of 90° rotation	Recapture into h=1113 bucket	V_{RF} increases before extraction
Longitudinal emittance $6\pi\sigma_\tau\sigma_E$	0.20 eV-sec	0.20 eV-sec	1.40 eV-sec	2.20 eV-sec	2.20 eV-sec	2.20 eV-sec
$\sqrt{6}\sigma_\tau$	1.34 ns	9.42 ns	65.9 ns	8.89 ns	8.89 ns	4.90 ns
$\sqrt{6}\sigma_E$ ($\sqrt{6}\sigma_E/E$)	47.6 MeV (3.15×10^{-4})	8.31 MeV (5.51×10^{-5})	8.31 MeV (5.51×10^{-5})	61.5 MeV (4.10×10^{-4})	61.5 MeV (4.08×10^{-4})	143 MeV (9.46×10^{-4})
V_{RF}	1.50 MV	2.30 kV	22 kV	22 kV	0.12 MV	1.0 MV
h	1113	1113	53	53	1113	1113
ν_s	2.24×10^{-3}	8.72×10^{-5}	5.91×10^{-5}	5.91×10^{-5}	1.24×10^{-3}	1.83×10^{-3}
Number per bunch	1.2×10^{10}	1.2×10^{10}	8.4×10^{10}	8.4×10^{10}	8.4×10^{10}	8.4×10^{10}
Microwave stability limit						
Z_L/n (broad band)	31.8 Ω	6.84 Ω	6.84 Ω	50.5 Ω	50.5 Ω	150 Ω
Z_{sh}/Q (narrow)	310 kΩ	9.45 kΩ	9.45 kΩ	74.0 kΩ	74.0 kΩ	399 kΩ

Table 12.2.2 Coalescence of 13 antiproton bunches at 150 GeV

	Start	V_{RF} lowered to match bunch	13 bunches in h=53 bucket	End of 90° rotation	Recapture into h=1113 bucket	V_{RF} increases before extraction
Longitudinal emittance $6\pi\sigma_\tau\sigma_E$	0.20 eV-sec	0.20 eV-sec	2.60 eV-sec	4.08 eV-sec	4.08 eV-sec	4.08eV-sec
$\sqrt{6}\sigma_\tau$	1.34 ns	9.42 ns	122 ns	8.89 ns	8.89 ns	6.68 ns
$\sqrt{6}\sigma_E$ $(\sqrt{6}\sigma_E/E)$	47.6 MeV (3.15×10^{-4})	8.31 MeV (5.54×10^{-5})	8.31 MeV (5.54×10^{-5})	114 MeV (7.61×10^{-4})	114 MeV (7.61×10^{-4})	195 MeV (1.29×10^{-3})
V_{RF}	1.50 MV	2.30 kV	22 kV	22 kV	0.46 MV	1.0 MV
h	1113	1113	53	53	1113	1113
ν_s	2.34×10^{-3}	8.72×10^{-5}	5.91×10^{-5}	5.91×10^{-5}	1.24×10^{-3}	1.83×10^{-3}
Number per bunch	8×10^{9}	8×10^{9}	1.04×10^{11}	1.04×10^{11}	1×10^{11}	1×10^{11}
Microwave instability limit						
Z_L/n (broad band)	47.8 Ω	10.3 Ω	10.3Ω	141 Ω	141 Ω	318 Ω
Z_{sh}/Q (narrow)	323 kΩ	14.0 kΩ	14.0 kΩ	204 kΩ	240 kΩ	620 kΩ

Table 12.2.3 RF maneuvering of proton bunches for $\bar{p}$ production

	120 GeV flat top	V_{RF} reduced and bunch rotates to max time spread	V_{RF} raised to 4 MV bunch rotates for 90^{o}
Longitudinal emittance $6\pi\sigma_\tau\sigma_E$	0.2 eV-sec	0.2 eV-sec	0.2 eV-sec
$\sqrt{6}\sigma_\tau$	1.11 ns	4.02 ns	0.31 ns
$\sqrt{6}\sigma_E$ $(\sqrt{6}\sigma_E/E)$	57.4 MeV (4.74×10^{-4})	15.8 MeV (1.31×10^{-4})	208 MeV (1.72×10^{-3})
V_{RF}	4 MV	300 kV	4 MV
Bucket height	314 MeV	85.4 MeV	314 MeV
ν_s	0.00405	0.00112	0.00405
Number per bunch	2.4×10^{10}	2.4×10^{10}	2.4×10^{10}
Microwave stability limit			
Z_L/n (broad band)	23.9 Ω	6.61 Ω	86.7
Z_{sh}/Q (narrow resonance)	281 kΩ	21.4 kΩ	3.69 MΩ

Mode	Resonance frequency (GHz)	Transit factor T	$(Z_{sh}/Q)/T$ (Ω)	Z_{sh}/Q (Ω)
p = 0	1.603 (1.57)	0.030	250	6.16 (2.38)
p = 1	1.919 (1.84)	0.202	254	51.3 (37.0)
p = 2	2.481 (2.42)	0.232	111	25.6 (24.3)
p = 3	3.261 (3.14)	0.242	48.7	11.8 (28.9)

Table 12.3.1 The four lowest resonance modes of a Main Ring bellow housing approximated as a closed pill box. The fifth column shows Z_{sh}/Q without consideration of transit-time effect. Results of numerical computations using TBCI and URMEL are enclosed in brackets.

Mode	Resonance frequency (GHz)	Quality factor	Z_{sh}/Q for 216 monitors (kΩ)
m = 1	1.28	1260	6.9
m = 3	3.84	2190	2.3
m = 5	6.40	2830	1.4
m = 7	9.00	3340	1.0

Table 12.3.2 The lowest resonance modes of 216 Main Ring beam monitors estimated as cylindrical strip plates.

	Low frequency $\lvert\bar{Z}_L/n\rvert$	High frequency Z_L/n or Z_{sh}/Q
Resistive wall	1.10 ohms	
Bellow Systems	2.46 ohms	Z_{sh}/Q = 37 kΩ
Beam monitors	0.32 ohms	Z_{sh}/Q = 6.9 kΩ
Kickers	0.03 ohms	
Lambertsons	0.81 ohms	Z_L/n = 0.35 ohms
Total	4.72 ohms	
Estimated limits	7.2 ohms	Z_L/n = 6.6 Ω Z_{sh}/Q = 9.5 kΩ

Table 12.3.3 Various contributions to the longitudinal impdedance of the Main Ring. $\lvert\bar{Z}_L/n\rvert$ is an average of Z_L/n over the bunch spectrum. This quantity will drive the single bunch coupled-mode instabilities. The high frequency contributions will drive the microwave instabilities. The limit Z_L/n occurs during preparation for p-production while the limit Z_{sh}/Q occurs during p-bunch coalescence. See Section 12.3 for details.

Frequency (MHz)	Q	Z_{sh} (kΩ)	Z_{sh}/Q (Ω)
1820 (1570)	183	0.269	1.47 (2.4)
2050 (1900)	1020	25.0	24.4 (37.0)
2536 (2400)	1000	29.7	29.7 (24.3)
3109 (3100)	1036	2.20	2.1 (28.9)
3188	708	1.35	1.9
3270	1090	2.2	2.0

Table 12.4.1 Wire measurement results of one bellow housing without sleeve pieces. The estimated values of Section 12.3 are included in brackets.

Frequency (MHz)	Q	Z_{sh} (kΩ)	Z_{sh}/Q (Ω)
794	53	2.4	45.0
1591	796	8.5	10.7
2103	280	2.7	9.8

(a)

Frequency (MHz)	Q	Z_{sh} (kΩ)	Z_{sh}/Q (Ω)
845	70	0.4	5.7
1685	337	3.9	11.6

(b)

Table 12.4.2 Wire measurement results of one beam monitor system (a) without sleeve pieces and (b) with sleeve pieces.

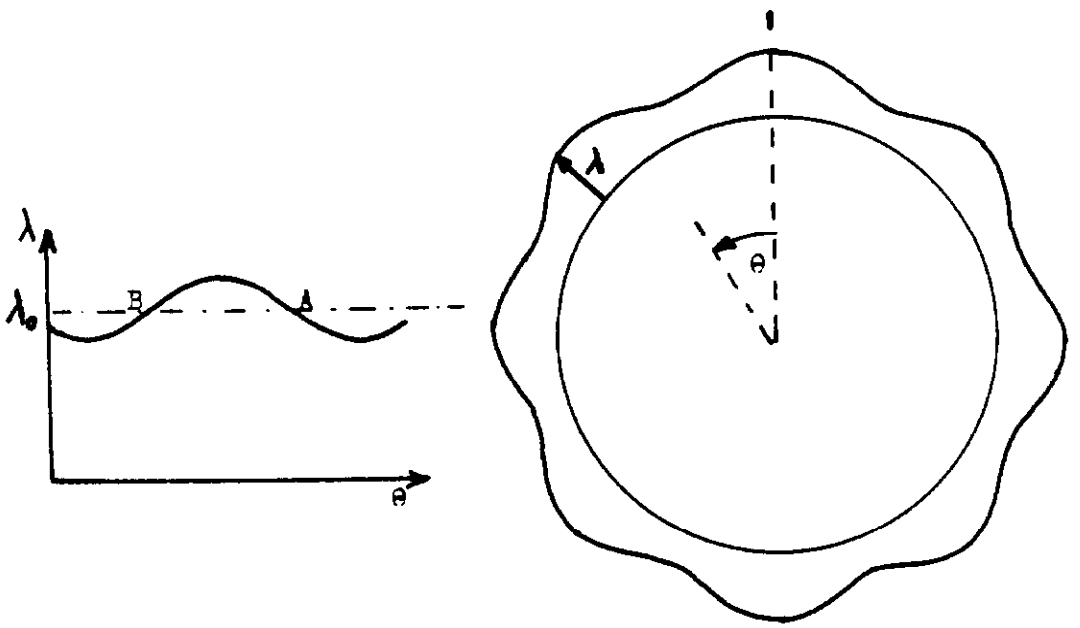

Figure 12.1.1 A perturbing longitudinal density wave. Space-charge force will increase the energy at the front of the wave crest A and decrease the energy at the back B.

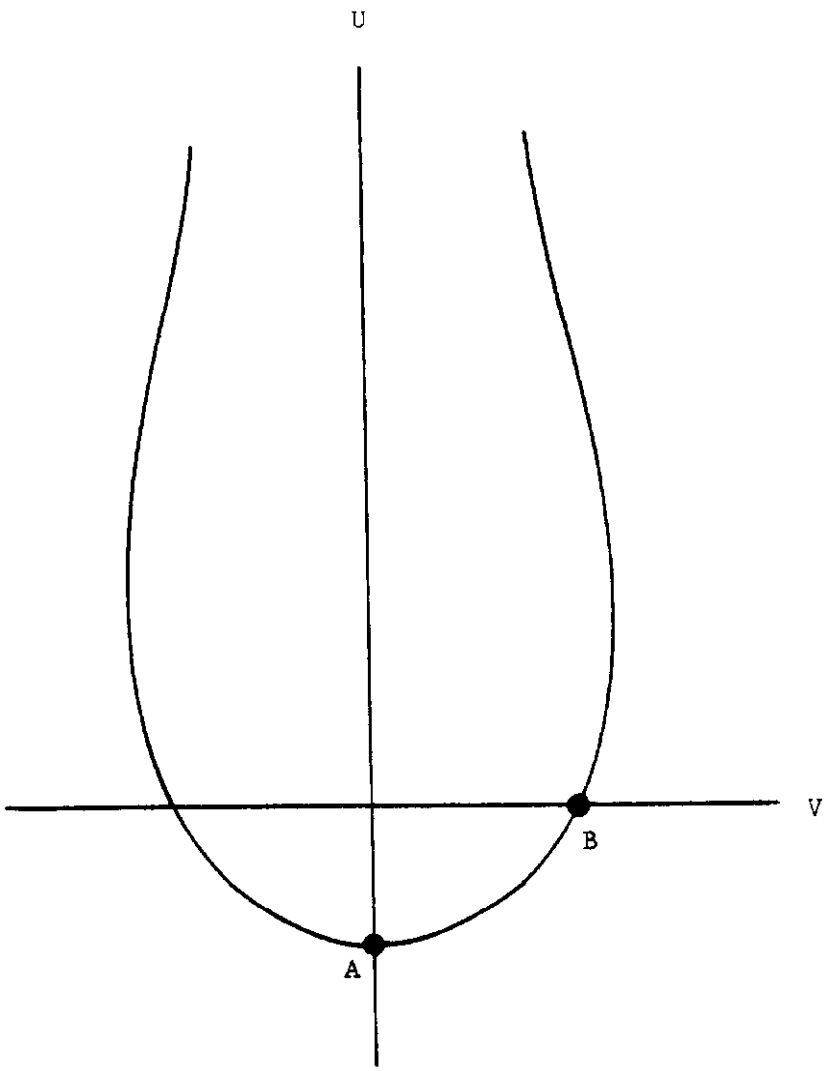

Figure 12.1.2 Stability curve of a Gaussian bunch in the $(\Delta\Omega_0/n)^2$-plane. V and U are the real and imaginary part of $(\Delta\Omega_0/n)^2$.

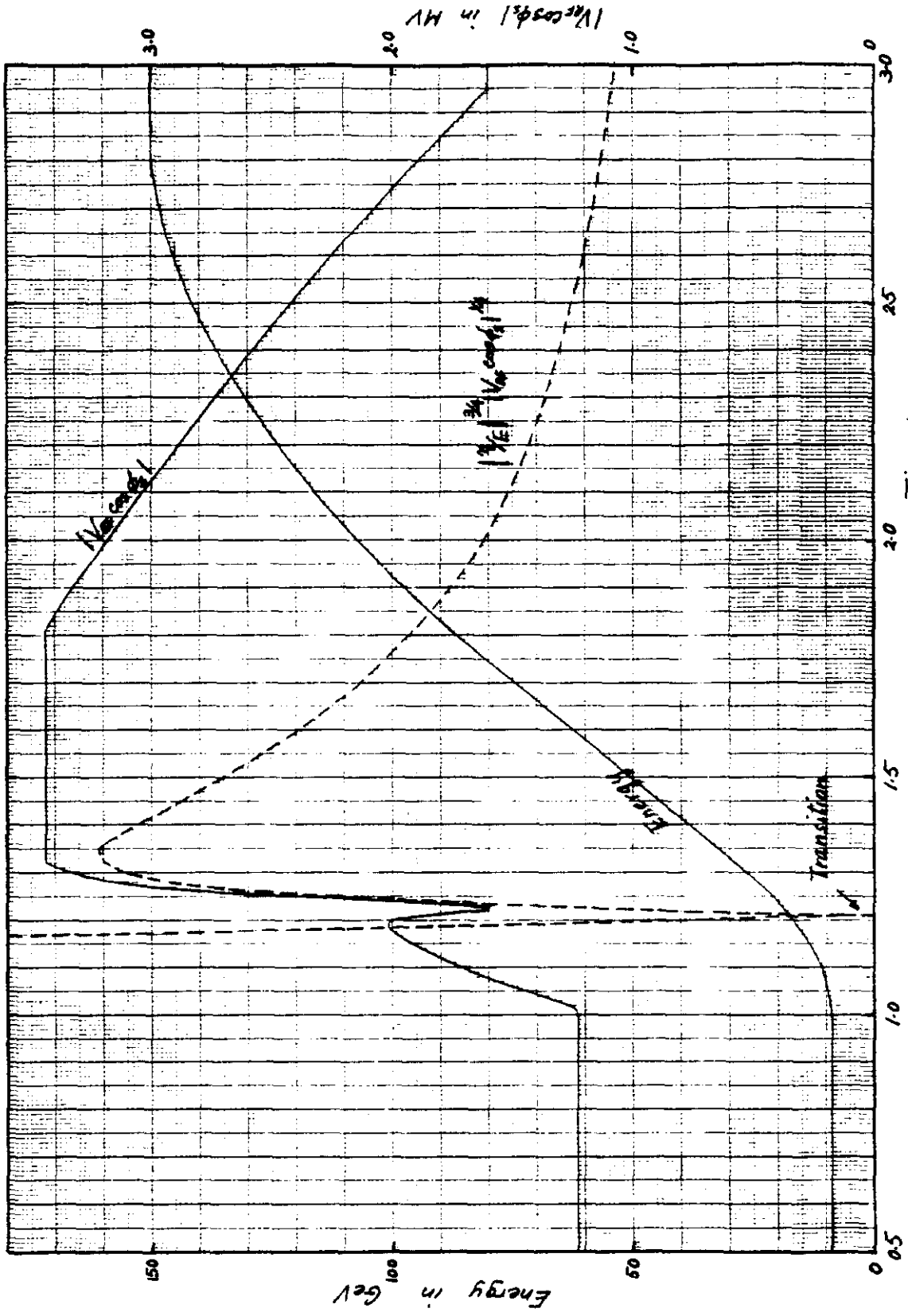

Figure 12.2.1 A typical acceleration cycle in the Main Ring. The scale of the dashed curve is arbitrary.

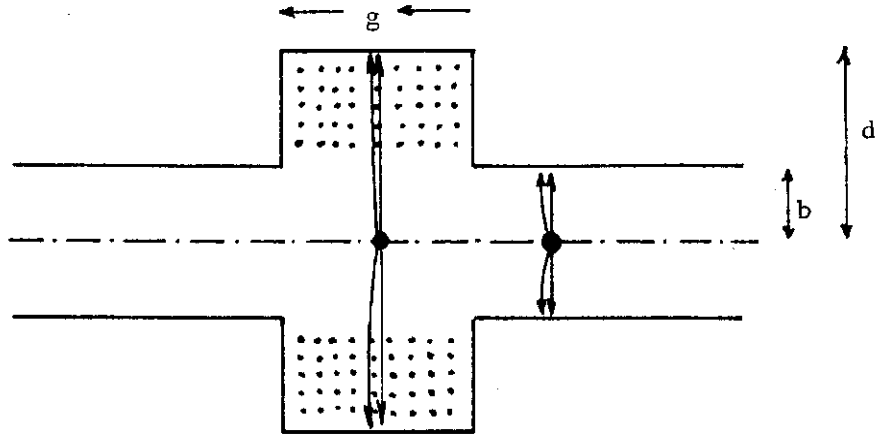

(a)

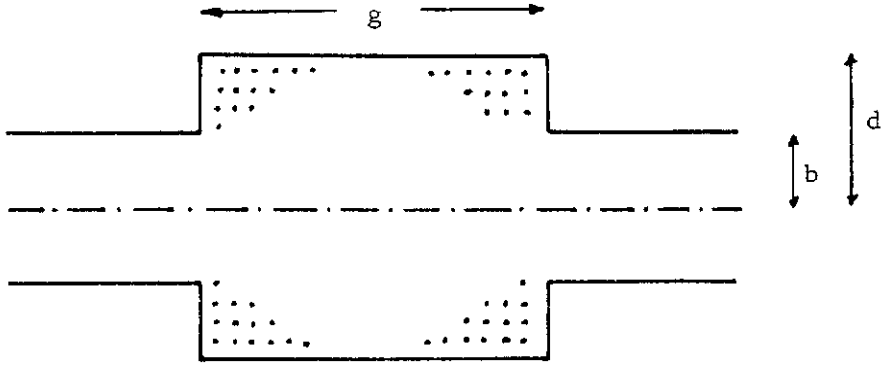

(b)

Figure 12.3.1 (a) Low frequency magnetic flux (dots) is trapped in the pill box after the passage of a particle whose electric fields are shown as solid arrows. (b) When $g \gg 2(d-b)$, only the flux near the corners is trapped; the flux in the middle leaks away.

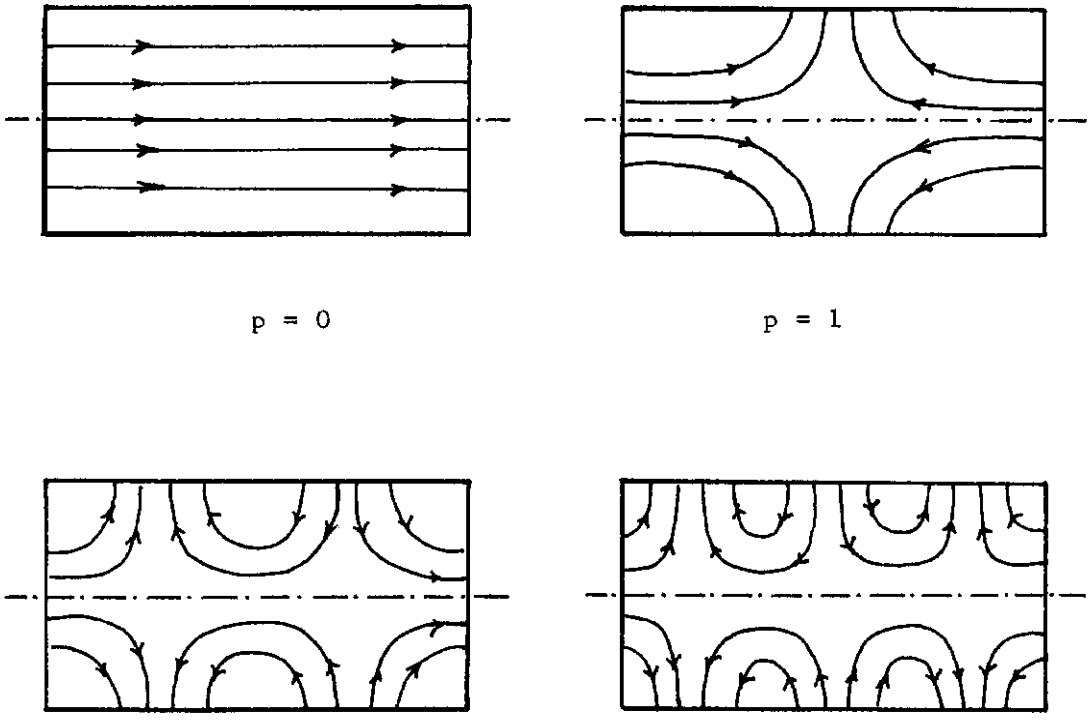

Figure 12.3.2 Electric field configurations inside a closed pill box (an approximation of the bellow housing) for the four lowest modes.

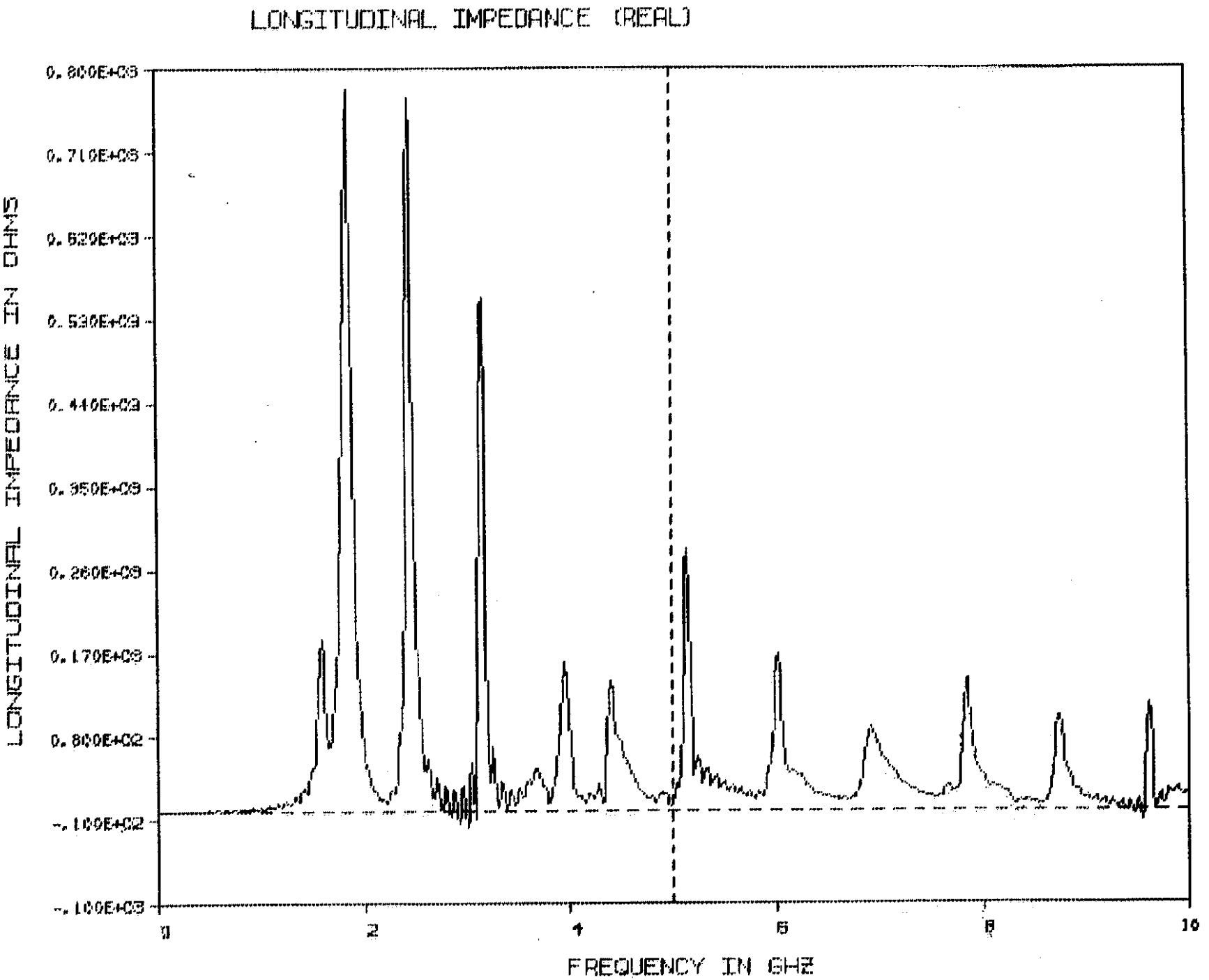

Figure 12.3.3 The first four resonance modes of a bellow system computed through TBCI.

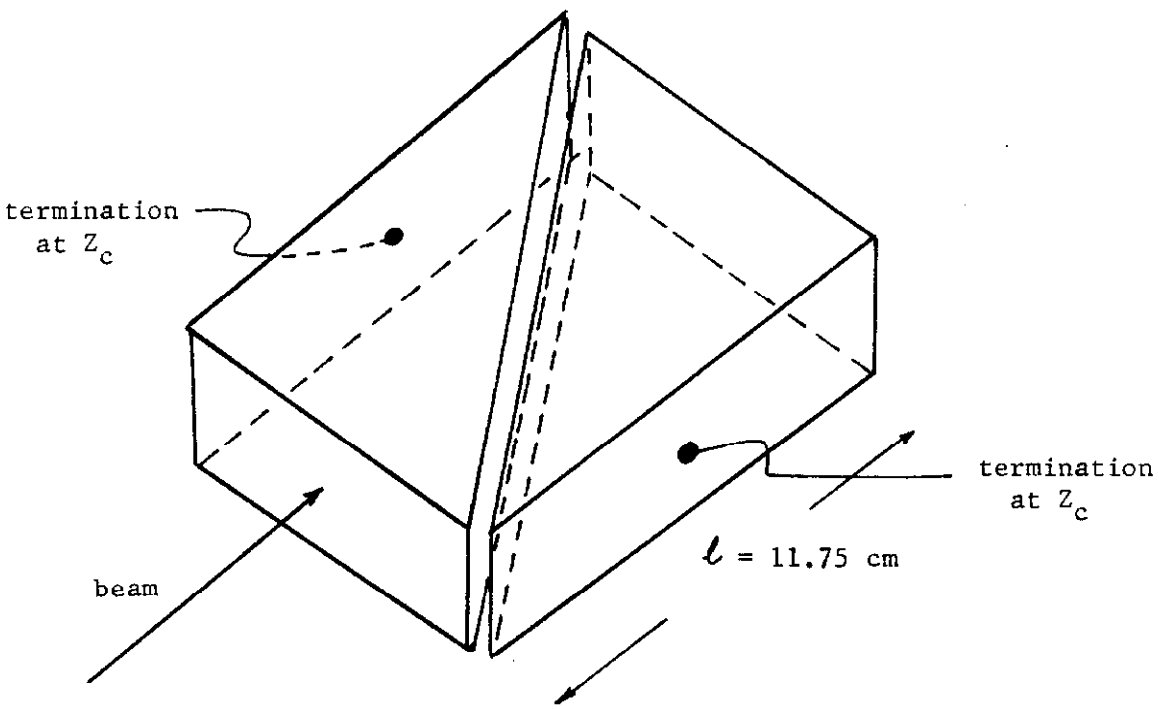

(a)

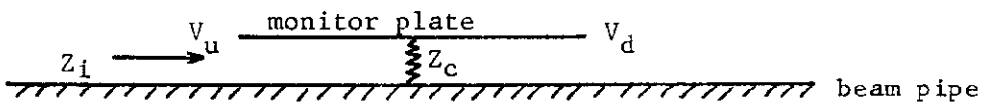

(b)

Figure 12.3.4 (a) A horizontal beam monitor.

(b) A monitor plate is terminated at middle by Z_c. A beam sees a voltage V_u and one V_d at the upstream and downstream ends.

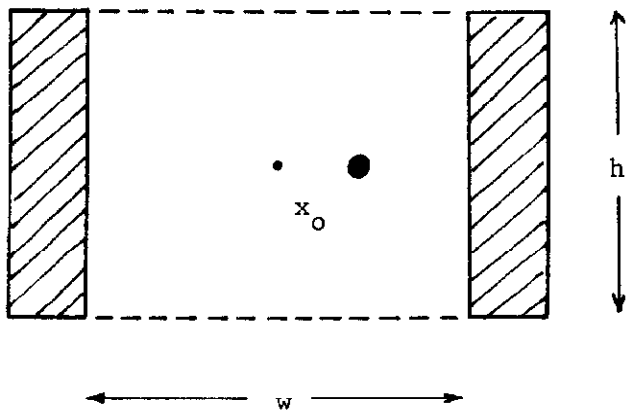

Figure 12.3.5 The cross section of a window magnet showing the beam deviating from the center by a distance x_o. The magnet current element is cross-hedged.

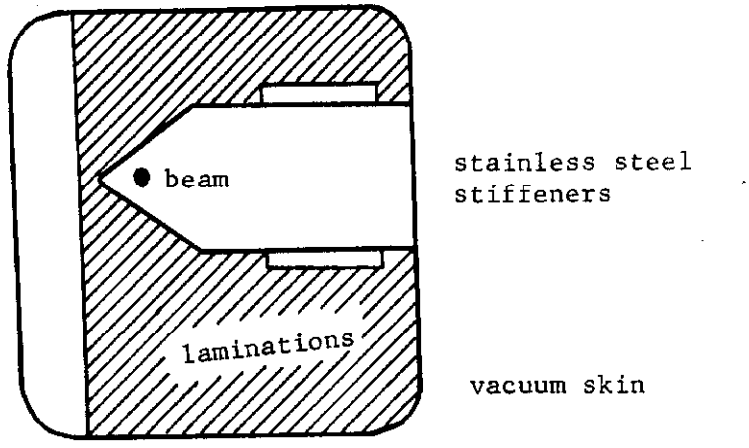

(a)

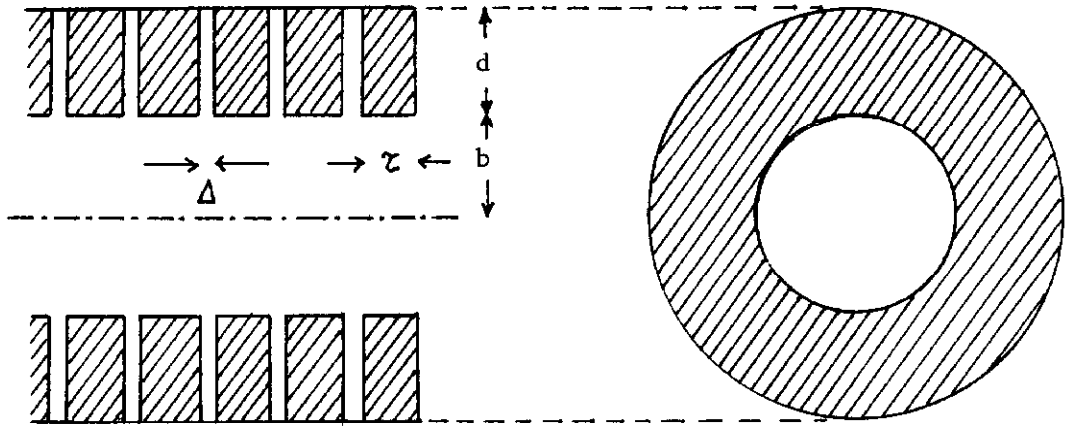

(b)

Figure 12.3.6 (a) The cross section of a Lambertson magnet.

(b) Approximation of the cross section of a Lambertson by an annular ring shorted at the outer circumference.

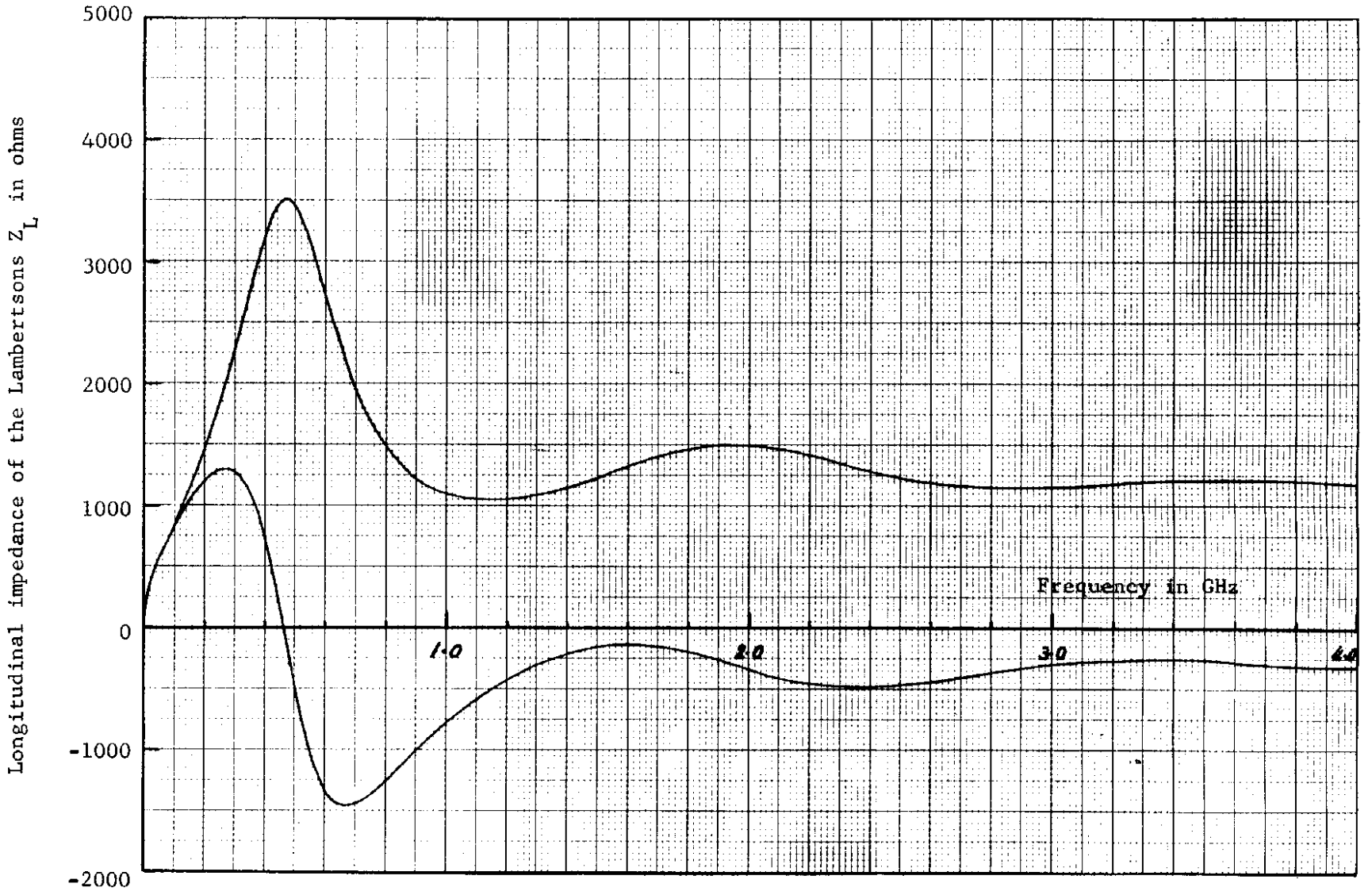

Figure 12.3.7 Estimated longitudinal impedance of the Lambertsons as a function of frequency. The upper curve is the real part and the lower curve the imaginary part.

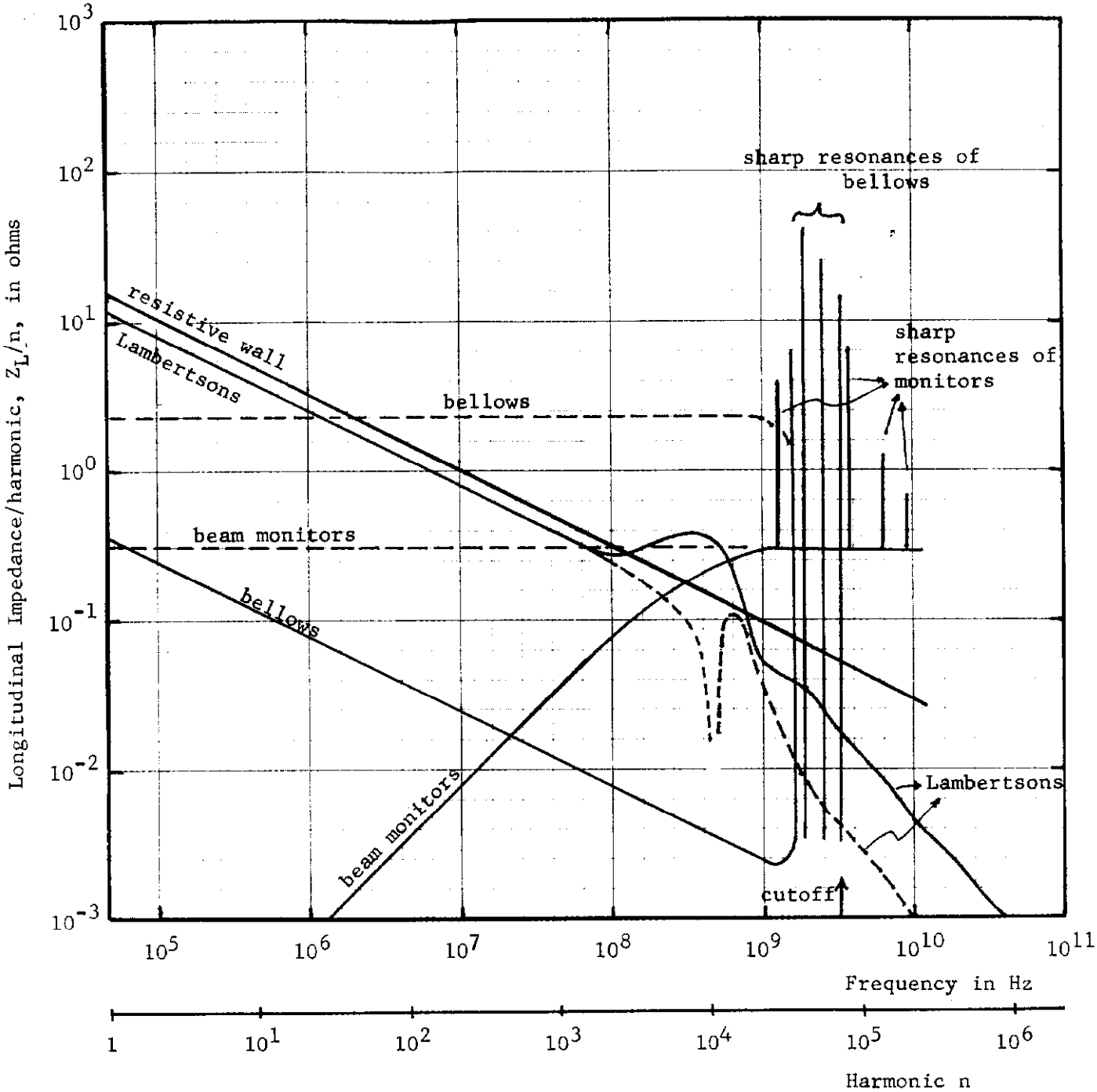

Figure 12.3.8 Various contributions to the longitudinal impedance/harmonic Z_L/n of the Main Ring. Solid curves represent the real parts and dashed curves represent the imaginary parts.

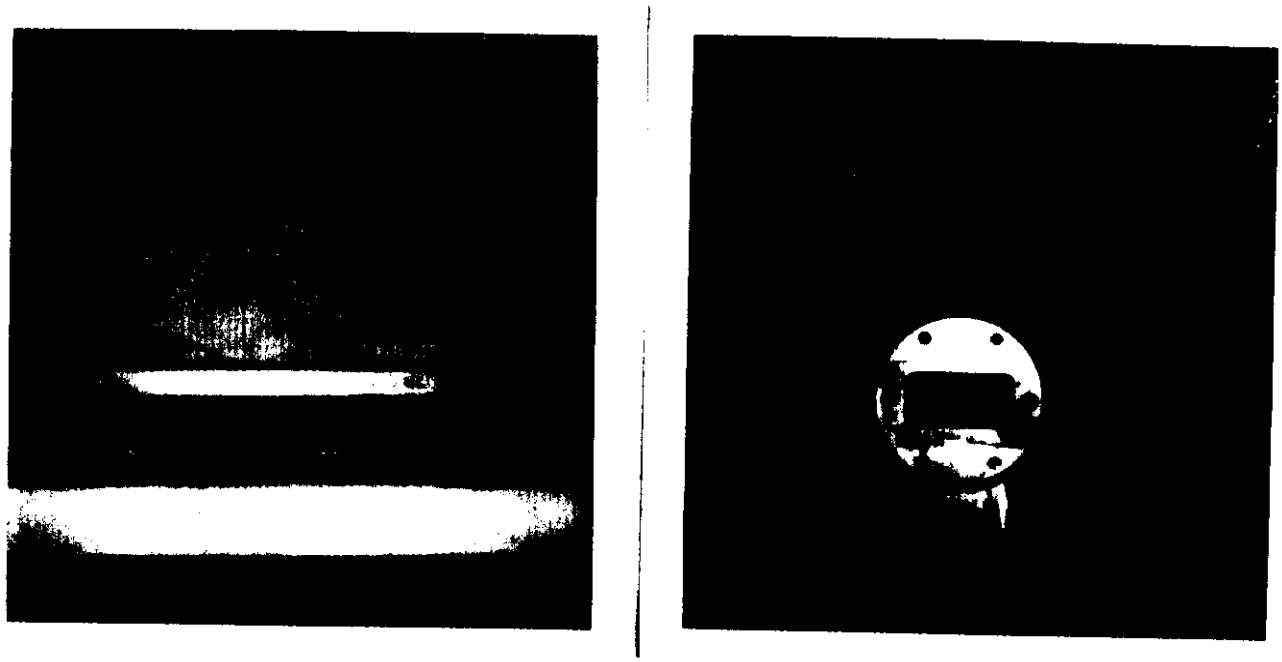

(a) (b)

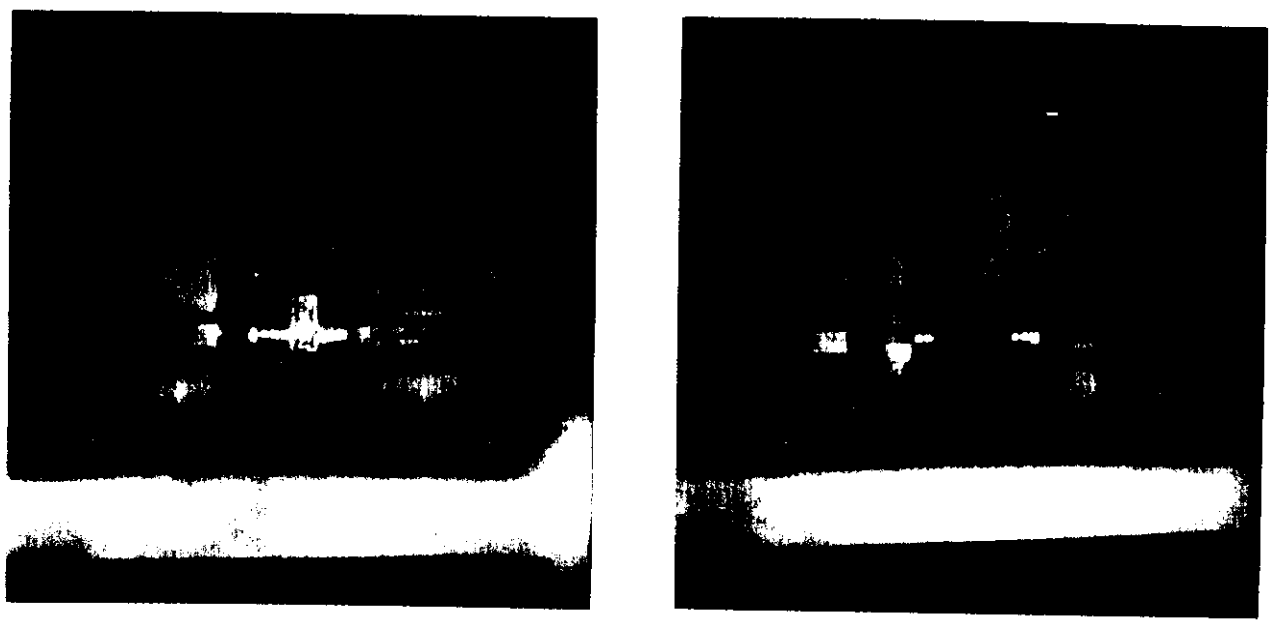

(c) (d)

Figure 12.4.1 Beam pipe sections to be tested. (a) Pipe A: a section of the the standard beam pipe to be used as a reference. (b) An end view of Pipe A. (c) Pipe B (or C): the standard beam pipe containing a typical bellow housing without (or with) sleeve pieces. (d) Pipe D: the standard beam pipe containing a beam monitor system with or without sleeve pieces.

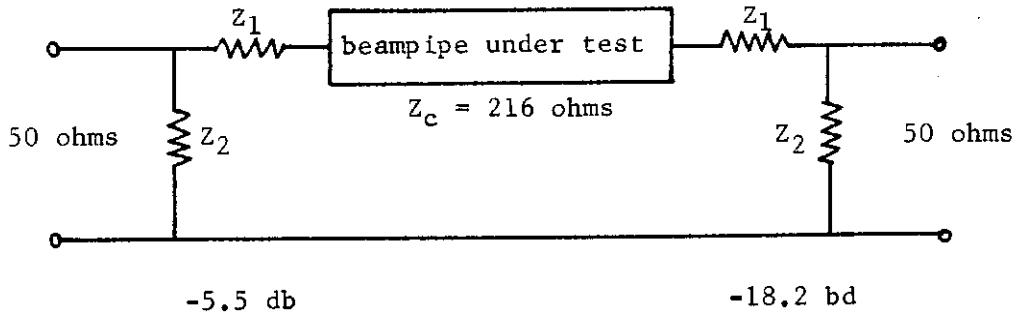

Figure 12.4.2a Circuit diagram matching network.

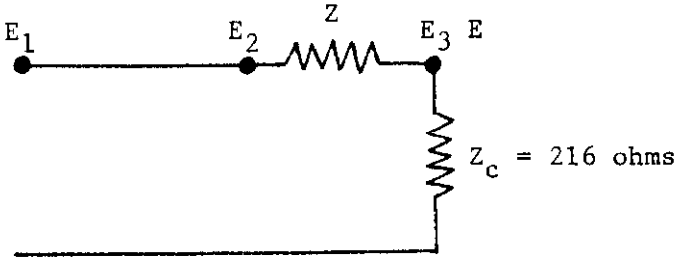

Figure 12.4.2b Voltage attenuation along the beam pipe due to a discontinuity impedance Z. The voltage E_2 before the discontinuity is equal to the incident voltage E_1 plus a reflected voltage ρE_1, where ρ is the reflection coefficient.

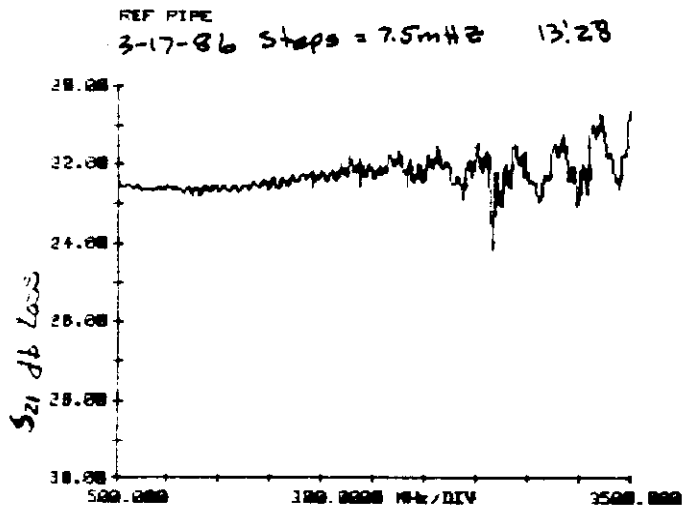

Figure 12.4.3 The attenuation as a function of frequency for the reference Pipe A. The nearly frequency independent curve indicates the excellent matching of the reference pipe to the 50 ohm cables. Note that the attenuation is very close to the designed value of -23.7 db.

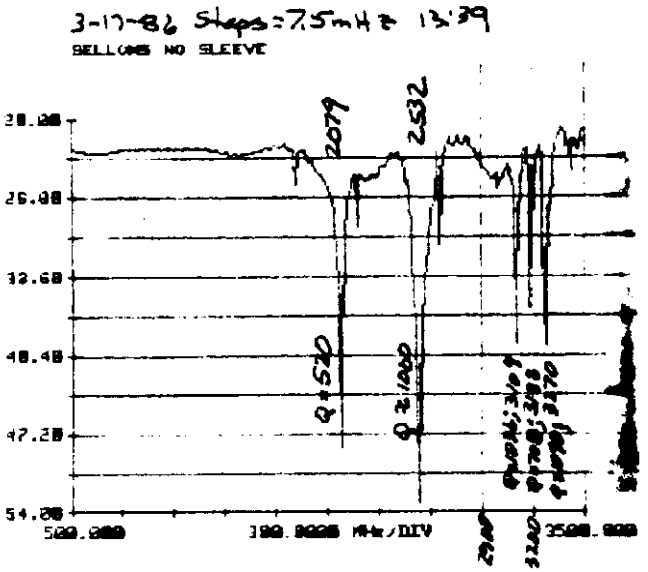

(a)

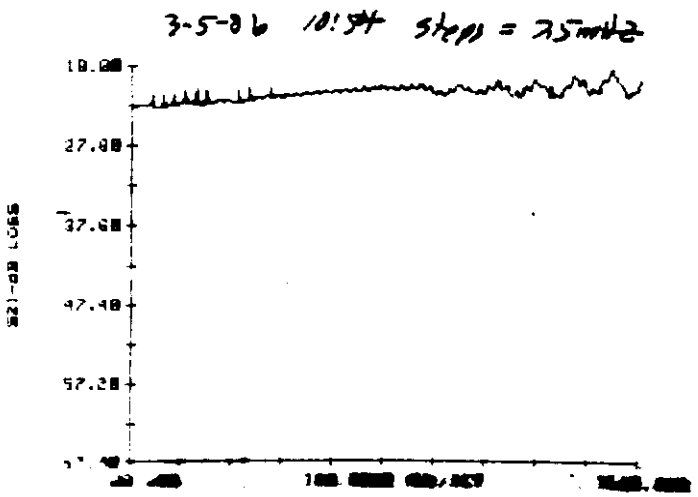

(b)

Figure 12.4.4 Wire measurement results of one bellow system (a) without sleeve pieces and (b) with sleeve pieces.

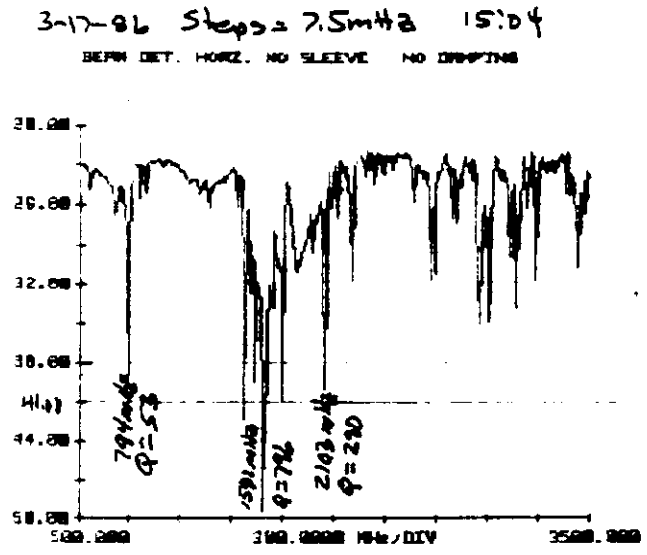

(a)

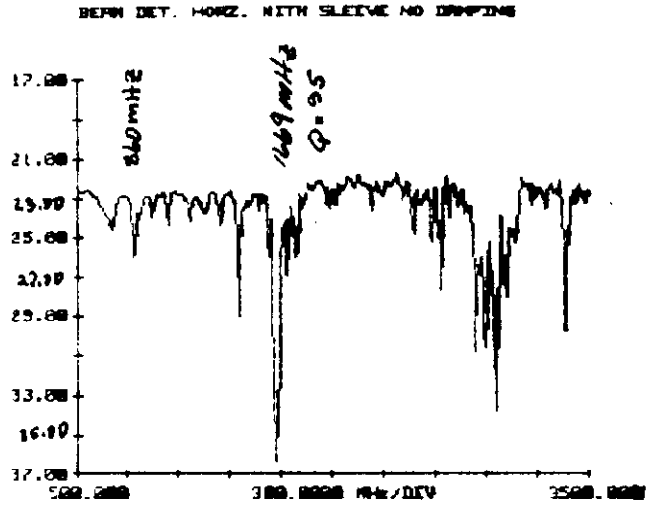

(b)

Figure 12.4.5 Wire measurement results of one beam monitor system (a) without sleeve pieces and (b) with sleeve pieces.

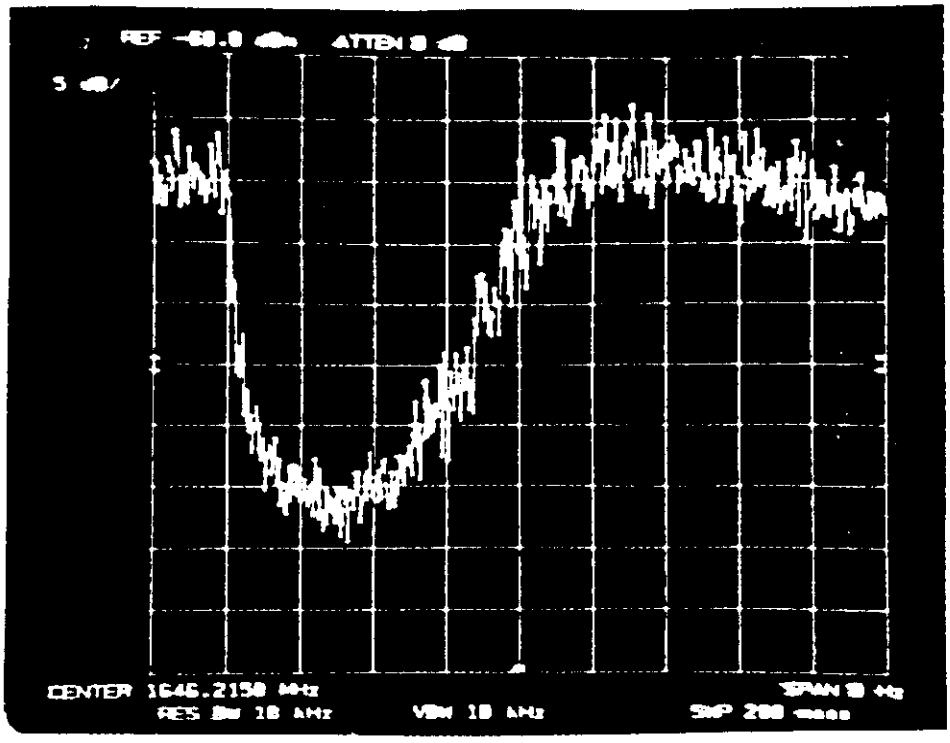

(a) Zero span mode 10 MHz bandwidth analyzer. Scales are 5db/div and 20ms/div.

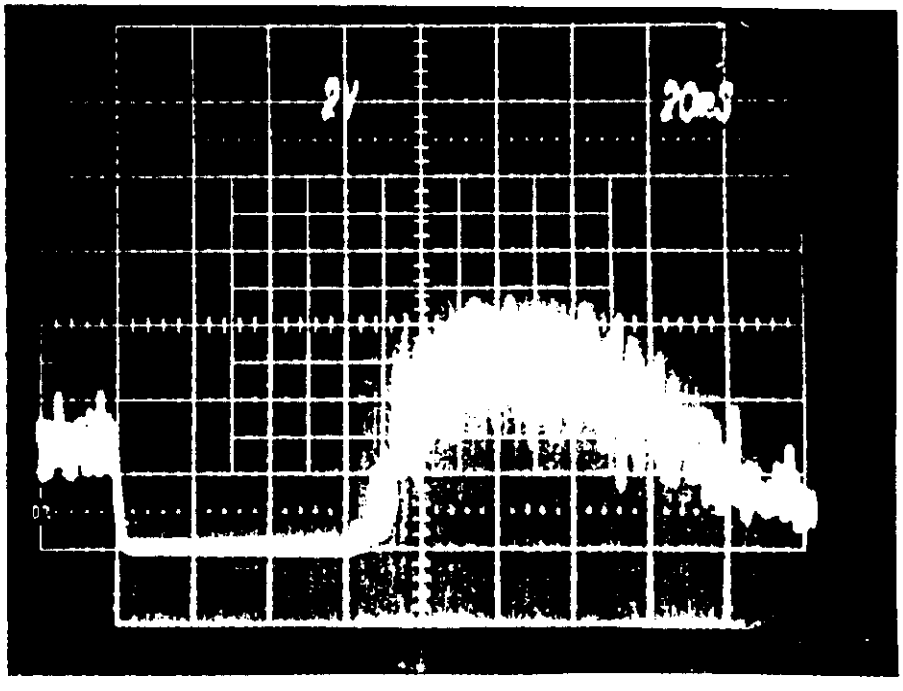

(b) Diode detector. Scales are 2V/div and 20ms/div.

Figure 15.5.1 Comparison of the starting growth times by zero-span analyzer and diode detector

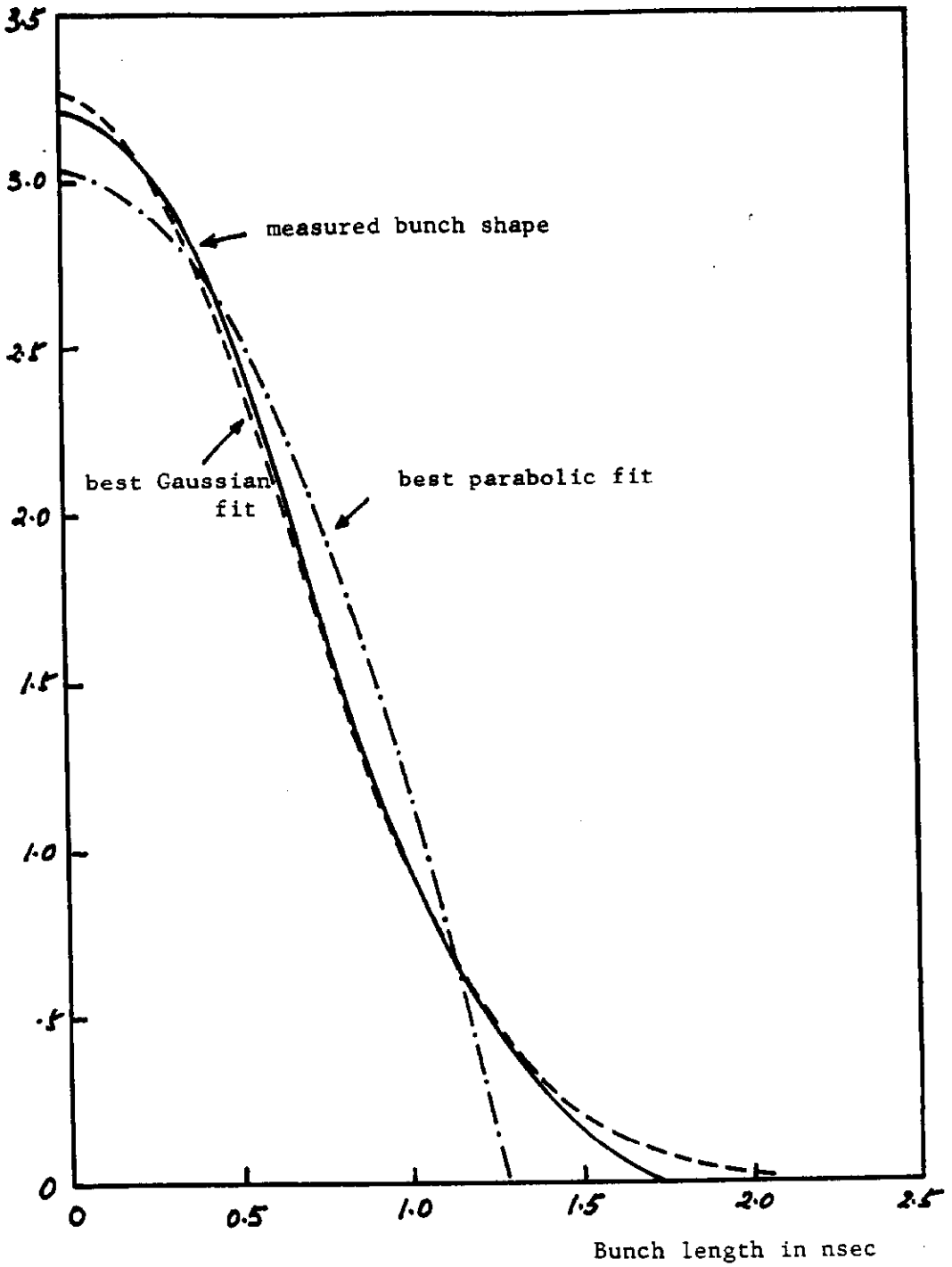

Figure 12.5.2 Bunch shape fittings. Solid curve is the measured bunch shape. Dot-dashed curve is the best parabolic fit with half bunch length = 1.278 nsec. Dashed curve is the best Gaussian fit with RMS time spread $\hat{\sigma}_z = 0.635$ nsec.

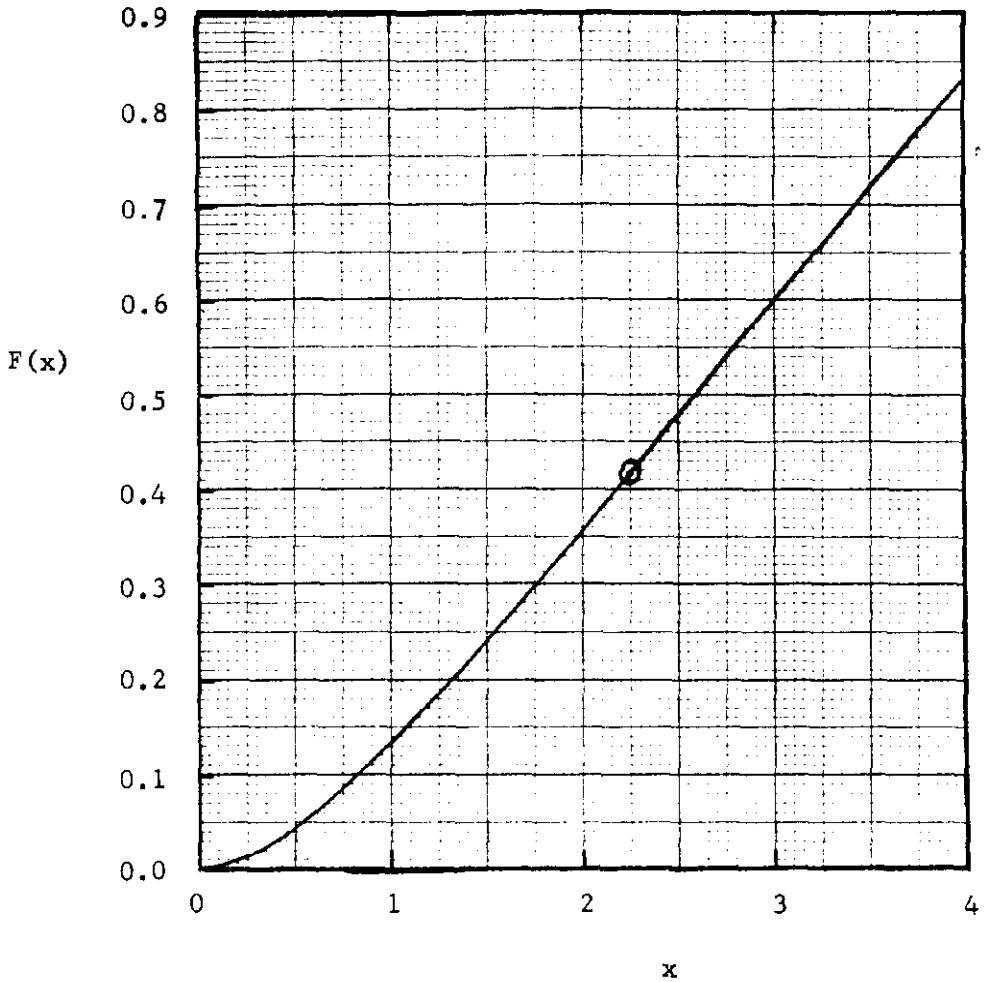

Figure 12.5.3 The normalized integrated growth rate F(x) of Eq. (4.5). The turning point is at x = 2.25 where the slope is 0.2194 .

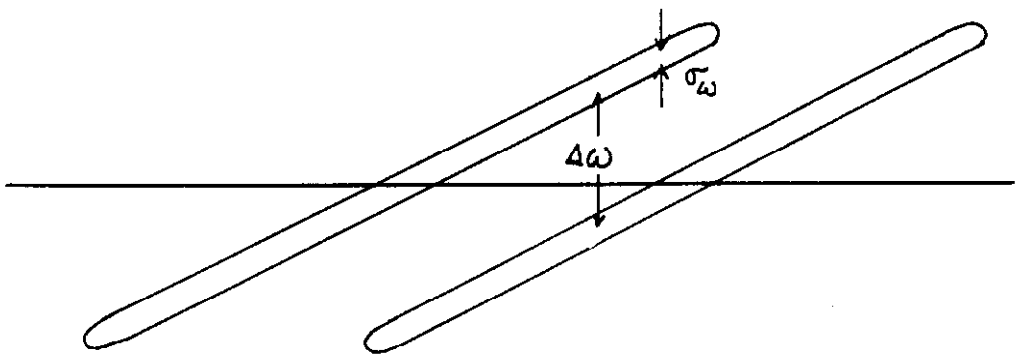

Figure 12.5.4 Two adjacent bunches overlap each other during debunching. Note that the frequency spread of each bunch σ_ω is very much less than the mean revolution frequency difference $\Delta\omega$ for particles in the two bunches at some azimuthal position.

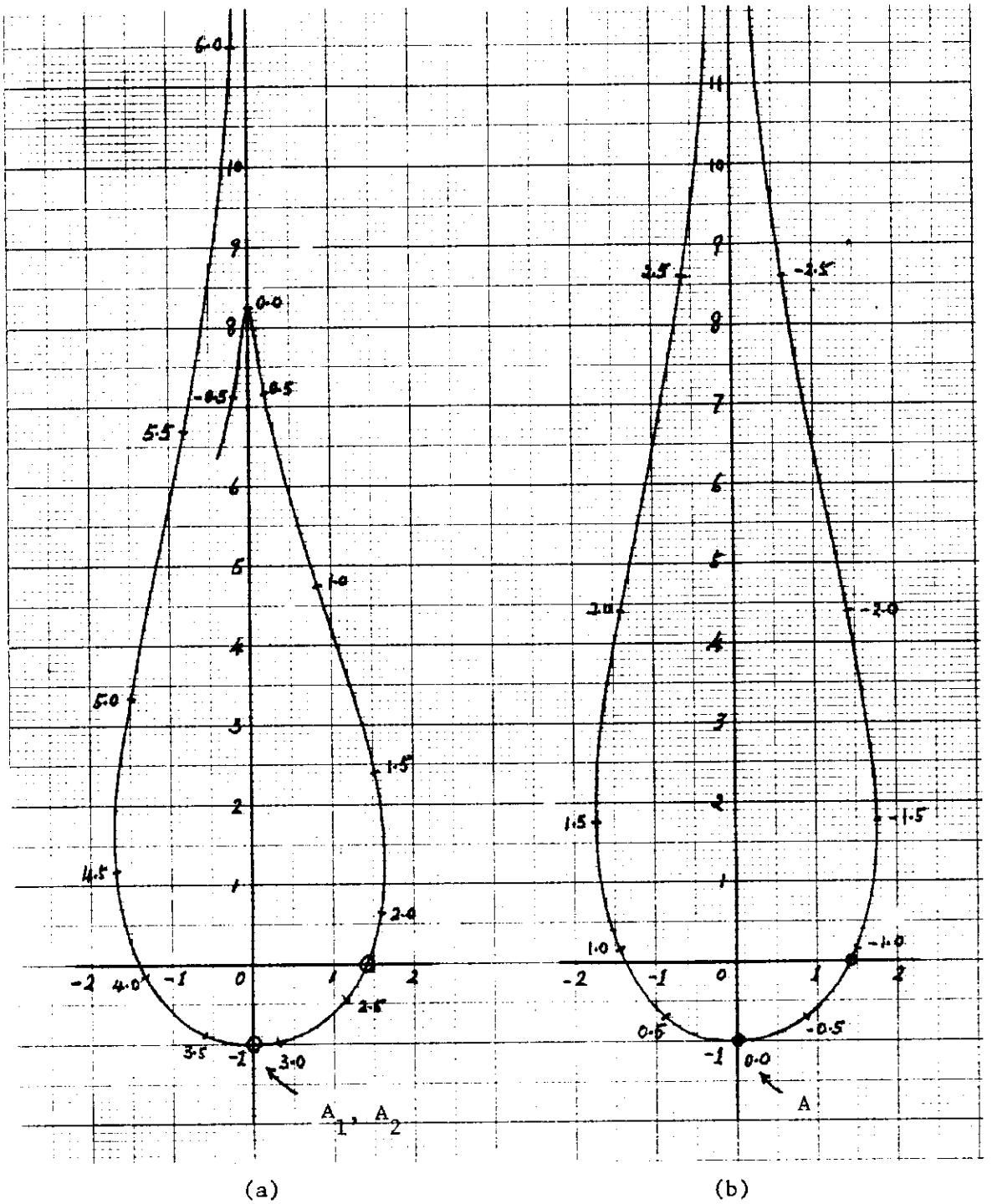

Figure 12.5.5 Threshold curves for (a) two overlapped bunches and (b) a single bunch. In each case, the abscissa and ordinate are the real and imaginary parts of $(\Delta\Omega_o/n\sigma_\omega)^2$ respectively. The real coherent frequency shift $Re(\Delta\Omega/\sqrt{2}n\sigma_\omega)$ is marked along the curves. For (a), because of clarity, only half of the curve is plotted.